NASA MEMO 12-23-58A

NASA

MEMORANDUM

THE STATIC AND DYNAMIC-ROTARY STABILITY DERIVATIVES OF A MODEL OF THE X-15 RESEARCH AIRPLANE AT MACH NUMBERS FROM 1.55 TO 3.50

By Phillips J. Tunnell and Eldon A. Latham

Ames Research Center
Moffett Field, Calif.

NATIONAL AERONAUTICS AND SPACE ADMINISTRATION

WASHINGTON

January 1959

[redacted]

NATIONAL AERONAUTICS AND SPACE ADMINISTRATION

MEMORANDUM 12-23-58A

THE STATIC AND DYNAMIC-ROTARY STABILITY DERIVATIVES OF A MODEL OF THE X-15 RESEARCH AIRPLANE AT MACH NUMBERS FROM 1.55 TO 3.50*

By Phillips J. Tunnell and Eldon A. Latham

SUMMARY

The static and dynamic stability derivatives of a 0.09-scale model of the X-15 research airplane have been determined by wind-tunnel tests and are presented herein. Tests were conducted at Mach numbers of 1.55, 2.00, 2.50, 3.00, and 3.50 at a Reynolds number of 1.5×10^6, based on the wing mean aerodynamic chord, at angles of attack from -6° to $+14^\circ$. Measurements were made of the damping-in-pitch, -yaw, and -roll derivatives, the cross derivatives, the static longitudinal and directional derivatives, and the effective dihedral derivative.

The complete model was statically stable both longitudinally and directionally throughout the test Mach number and angle-of-attack range. In general, the addition of speed brakes increased the directional stability and the damping in yaw, the higher the Mach number, the greater the increase. The modification of the vertical tail from an 11.5° double-wedge section to a 10° single-wedge section of 5 percent less area provided an appreciable increase in directional stability and damping in yaw at Mach numbers of 2.5, 3.0, and 3.5.

INTRODUCTION

An understanding of the damping derivatives, as well as the static forces acting on an airplane, is very important in the design of high-speed aircraft. To further this understanding, tests were conducted in the Ames Unitary Plan wind tunnel to measure the rotary derivatives of an advanced model of the X-15 research airplane. A model of an earlier version of this airplane was tested in the 8- by 7-foot test section of the Ames Unitary Plan wind tunnel at Mach numbers of 2.50, 3.00, and 3.50.

[redacted]

[redacted]

The results of this earlier test are reported in reference 1 and, where the data are comparable, they are presented in the summary curves of this report. Also presented in the summary curves are some of the results of a subsonic test program conducted in the Ames 12-foot pressure wind tunnel in which the same advanced model was used.

The purpose of this report is to present experimental data obtained by wind-tunnel oscillation tests and to compare these data with theoretical estimations and other test results. The derivatives obtained from this test are referred to a body system of axes and include the following: static longitudinal stability $\left(C_{m_\alpha}\right)$, damping in pitch $\left(C_{m_q} + C_{m_{\dot{\alpha}}}\right)$, damping in roll $\left(C_{l_p} + C_{l_{\dot{\beta}}} \sin \alpha\right)$, rolling moment due to yawing $\left(C_{l_r} - C_{l_{\dot{\beta}}} \cos \alpha\right)$, damping in yaw $\left(C_{n_r} - C_{n_{\dot{\beta}}} \cos \alpha\right)$, yawing moment due to rolling $\left(C_{n_p} + C_{n_{\dot{\beta}}} \sin \alpha\right)$, rolling moment due to sideslip $\left(C_{l_\beta}\right)$, and static directional stability $\left(C_{n_\beta}\right)$.

NOTATION

Moments and deflections are referred to a body system of axes (fig. 1). The various stability derivatives are defined as follows:

C_{m_α} $\dfrac{\partial C_m}{\partial \alpha}$

$C_{m_{\dot{\alpha}}}$ $\dfrac{\partial C_m}{\partial(\dot{\alpha}\bar{c}/2V)}$

C_{m_q} $\dfrac{\partial C_m}{\partial(q\bar{c}/2V)}$

C_{n_β} $\dfrac{\partial C_n}{\partial \beta}$

$C_{n_{\dot{\beta}}}$ $\dfrac{\partial C_n}{\partial(\dot{\beta}b/2V)}$

C_{n_r} $\dfrac{\partial C_n}{\partial(rb/2V)}$

C_{n_p} $\dfrac{\partial C_n}{\partial(pb/2V)}$

C_{l_p} $\dfrac{\partial C_l}{\partial(pb/2V)}$

C_{l_β} $\dfrac{\partial C_l}{\partial \beta}$

$C_{l_{\dot{\beta}}}$ $\dfrac{\partial C_l}{\partial(\dot{\beta}b/2V)}$

C_{l_r} $\dfrac{\partial C_l}{\partial(rb/2V)}$

Additional symbols are as follows:

C_m pitching-moment coefficient, $\dfrac{\text{pitching moment}}{(1/2)\rho V^2 S\bar{c}}$

C_n yawing-moment coefficient, $\dfrac{\text{yawing moment}}{(1/2)\rho V^2 Sb}$

C_l rolling-moment coefficient, $\dfrac{\text{rolling moment}}{(1/2)\rho V^2 Sb}$

a single data point

$\bar{a}$ averaged data point

b wing span

$\bar{c}$ mean aerodynamic chord

M Mach number

n number of data points at a single test condition

V free-stream velocity

q pitching velocity, radians/sec

r yawing velocity, radians/sec

p rolling velocity, radians/sec

S total wing area

α angle of attack, radians except where noted

β angle of sideslip, radians except where noted

δ_h horizontal-tail incidence angle, deg (positive deflection indicated in fig. 1)

ρ density

Subscripts

w wing

v vertical tail

h horizontal tail

MODEL

A 0.09-scale model of the X-15 research airplane was supplied by North American Aviation, Incorporated, for this investigation. A list of model geometry is presented in table I, and a three-view sketch is shown in figure 2. Photographs of the model installed in the tunnel are shown in figure 3.

The model was constructed specifically for oscillation testing which requires that the model be light to keep inertial forces low. To achieve this requirement, the construction was entirely of plastic laminated glass cloth and magnesium. Other features of the model included an adjustable incidence angle of the horizontal tail and removable tail surfaces. When the tail surfaces were removed they were replaced with fairings set flush to the fuselage. Speed brakes that attached to the vertical tails were also provided.

The subject model was a modification of a model tested previously in the 8- by 7-foot test section of the Ames Unitary Plan wind tunnel and is described in reference 1. The modification consisted of decreasing the length of the fuselage fairings as shown by the dashed line in figure 2, and of replacing the 11.5° double-wedge tail section symmetrically disposed about the fuselage center line with a 10° single-wedge tail section of asymmetrical shape and 5 percent less area.

APPARATUS

Tests were conducted in the 9- by 7-foot and 8- by 7-foot supersonic test sections of the Ames Unitary Plan wind tunnel. These two test sections provide Mach number variations from 1.55 to 3.50 at a constant Reynolds number. A more detailed description of the wind tunnel may be found in reference 2.

The oscillation test apparatus consisted of two dynamic balances and their associated electronic equipment. Basically, the dynamic balance supports the model on a set of crossed flexures, or springs, allowing the model to oscillate in a single degree of freedom about a fixed axis. The oscillation frequency varied from 4 to 8 cycles per second, depending on the aerodynamic moment. The data presented in this report were taken for a maximum peak oscillation amplitude of approximately 2°. A more detailed description of this apparatus and the technique used to measure the rotary derivatives is given in reference 3.

TESTS

Data were taken at Mach numbers of 1.55, 2.00, 2.50, 3.00, and 3.50 at a constant Reynolds number of 1.5 million, based on the mean aerodynamic chord of the wing. For most cases test points were taken from -6° to $+14^{\circ}$ angle of attack at 2° increments. The mean angle of sideslip was 0° throughout the tests.

The various configurations tested were as follows: complete airplane; complete airplane with speed brakes extended to 35°; complete airplane less vertical-tail surfaces for oscillation about the yaw axis; complete airplane less horizontal-tail surfaces for oscillation about the pitch axis; and complete airplane less both the vertical and horizontal tails. Horizontal-tail deflections of 5°, 0°, -5°, -10°, -15°, and -20° were used when necessary to keep the pitching moment within the allowable balance limits.

CORRECTIONS TO DATA

Corrections to the measured values of the damping coefficients due to internal damping of the oscillation mechanism were determined from wind-off measurements of the damping with tunnel evacuated to about 3 pounds per square inch absolute. These measurements were taken prior to each test to determine the corrections to be applied to the test data to produce a pure aerodynamic term.

[redacted]

ACCURACY OF DATA

Many factors can influence the accuracy of wind-tunnel data; however, for these tests the random error, as illustrated by the data scatter, was a good indication of the absolute error. All of the derivatives exhibited scatter with the rolling and cross derivatives showing the greatest error. As shown in figure 4, the average scatter increases considerably at angles of attack in excess of about 8°. It was noted that more scatter exists in the data from the 9- by 7-foot test section than from the 8- by 7-foot test section. The cause of this difference is unknown. The average scatter is defined as $\Sigma|a - \bar{a}|/n$. The scatter of the cross derivative data represents the worst case encountered. The remaining derivatives are believed to contain no more error than is indicated by the scatter on their respective curves.

PRESENTATION OF RESULTS

The results of this investigation are presented in the form of basic and summary data curves (figs. 5 through 15). These figures show the effect of model components on the aerodynamic derivatives. The basic curves show the results of this investigation as functions of angle of attack. The summary curves contain not only the supersonic results from these tests but also subsonic results from static- and dynamic-force tests of the identical model made in the Ames 12-foot pressure tunnel, (ref. 4). Also shown in the summary plots for comparison are results from tests of an earlier modification (ref. 1), in which the vertical tail was an 11.5° double-wedge section, symmetrically disposed about the body axis, and the fuselage fairings extended farther forward. Estimated values of the static and dynamic derivatives obtained by the method of reference 1 are presented in the summary curves. Summary plots of the variation of the cross derivatives with Mach number have been excluded. Since the model is nearly symmetrical, the cross derivatives are small and, in general, the average scatter was of the order of the average value of the derivative.

The results of this investigation are presented in the following figures:

	Figure
Longitudinal derivatives	
Static stability	5
Damping in pitch	5
Variation of static stability with Mach number	6
Variation of damping in pitch with Mach number	7
Yawing derivatives	
Damping in yaw	8
Rolling moment due to yawing	8
Variation of damping in yaw with Mach number	9

[redacted]

DISCUSSION

The results have been presented in the form of basic and summary data curves. These results, in general, corroborate the analysis made of an earlier version of the same airplane in reference 1. This discussion presents some pertinent observations regarding the effect of the modifications as well as general points of interest not brought out in the reference report.

In general, the data of different stabilizer settings could be faired; however, this could not be done at a Mach number of 3.5 with a -15° stabilizer setting, on the complete airplane with and without speed brakes (fig. 5). Data from unpublished static-force tests corroborate the trend of decreasing longitudinal static stability with increasing negative stabilizer settings at Mach numbers above 3.00 and at angles of attack above 8°. This effect can be attributed to the forward surface of the stabilizer being influenced at negative deflections by the pressure field from the wing and is a result of the close coupling of the wing and horizontal-tail surfaces.

Modification of the Fuselage Fairings

Decreasing the length of the fuselage fairings brought about distinct changes in the longitudinal derivatives with very little or no change to the lateral derivatives. This would be expected because of the loss of lifting surface forward of the point of moment reference. Figures 6 and 7 show a definite increase in the longitudinal stability and a small decrease in the damping in pitch at Mach numbers of 2.5, 3.0, and 3.5 at 0° angle of attack. In making the preceding comparison it was assumed that the vertical-tail modification had negligible effect on the longitudinal derivatives. For the case of the lateral derivatives $C_{n_r} - C_{n_{\dot{\beta}}} \cos \alpha$, $C_{l_p} + C_{l_{\dot{\beta}}} \sin \alpha$, C_{l_β}, and C_{n_β}, decreasing the length of the fuselage fairings had little or no effect at 0° angle of attack and at the

comparison Mach numbers, as shown in figures 9, 11, 13, and 15, respectively. Comparison of the present results for vertical tail off with those of the reference report indicates the effects of the fuselage fairings.

Modification of the Vertical Tail

The change in the tail shape favoring the upper tail coupled with the change in section from a double- to a single-wedge airfoil favorably affected the lateral derivatives at 0° angle of attack and at the comparison Mach numbers of 2.5, 3.0, and 3.5. Figure 13 shows the favorable effective dihedral increment due to the tail modification. For the complete airplane at Mach numbers above 2, the effective dihedral varied little with angle of attack as is shown in figure 12. With this particular distribution of vertical-tail area, the contribution of the horizontal-tail dihedral was just about offset by the change in effectiveness of the vertical tail due to the wing pressure field variation with angle of attack. At the lower Mach numbers (1.5 to 2.0) the vertical tail was not affected so greatly by the wing pressure field and hence experienced less change in effectiveness.

The 10° single-wedge section of the tail had 5 percent less total area than the 11.5° double-wedge section and any increase to the directional stability, as well as the damping in yaw, must be the result of an increase in the effectiveness of the single-wedge section compared to the double-wedge section. The increase in lift-curve slope of blunt trailing-edge airfoils at supersonic speeds is summarized in reference 5. An additional stability benefit is provided by a rearward shift in the center of pressure of the single-wedge vertical tail as compared to the double-wedge tail. Both of the derivatives, plotted in figures 9 and 15, show a considerable increase, illustrating greater stability in this speed range with the single-wedge section. As shown in figure 11, the damping in roll was also increased by the tail modification. However, the asymmetrical area distribution as well as the change in tail section contributed to the increase in this derivative.

Effect of Speed Brakes

The addition of speed brakes, in general, had a relatively minor influence on the longitudinal derivatives in the ranges of Mach numbers and angles of attack tested (fig. 5).

The yawing derivatives were the most affected by the speed brakes as would be expected because of their position. The directional stability was approximately doubled at a Mach number of 3.5 and 0° angle of attack

(fig. 14); however, at an angle of attack of 10° there was no benefit. In general, over the range of test Mach numbers, the maximum increase in directional stability due to speed brakes occurred near 0° angle of attack, and at angles of attack above or below 0° the benefit became less. This is shown in the following table:

M	α for maximum ΔC_{n_β}, deg	α for minimum ΔC_{n_β}, deg
1.55	3	-6 and +9
2.00	2	-6 and +12
2.50	-4	-6 and +10
3.00	-4	-6 and +14
3.50	-4	-6 and +12

This trend is reversed for damping in yaw, as shown in figure 8 and the following table; that is, the maximum increase in damping occurred at or near 10° angle of attack and the minimum increase occurred at about 0° angle of attack.

M	α for maximum $\Delta(C_{n_r} + C_{n_{\dot\beta}} \cos \alpha)$, deg	α for minimum $\Delta(C_{n_r} + C_{n_{\dot\beta}} \cos \alpha)$, deg
1.55	-6 and +10	2
2.00	-6 and +12	2
2.50	-6 and +10	0
3.00	-6 and +10	-4
3.50	-6 and +10	-3

The damping in roll of the basic configuration was stabilizing at all test conditions (see fig. 10); however, the addition of speed brakes had a varying effect on damping in roll.

The rolling moment due to sideslip was little affected by the addition of speed brakes at 0° angle of attack. At Mach numbers above 2.0 at high angles of attack however, the rolling moment due to sideslip was increased (fig. 12).

Estimated Derivatives

Values of the stability derivatives, calculated by the equations of reference 1, are presented in the summary figures for comparison with experimental data. These computations were made without a precise knowledge of the static aerodynamic forces on the model and, therefore, it has been necessary to make the following assumptions. For these estimates it was assumed that the effective area of a lifting surface was that

obtained by projecting the leading and trailing edges to the center of the fuselage. The downwash and sidewash at the tail were assumed to be zero, and the dynamic pressure acting on the tail surfaces was assumed to be the free-stream value. The consequences of using some of these assumptions cannot be readily ascertained without an accurate knowledge of the sidewash, downwash, and other details of the flow. In absence of data of this type, the calculated values presented on the summary curves of this report are intended to illustrate the degree of accuracy that can be obtained in estimating the rotary derivatives for this type of model.

SUMMARY OF RESULTS

A wind-tunnel investigation has been conducted at supersonic speeds to determine the static and dynamic-rotary stability derivatives of the X-15 research airplane. Data were obtained at Mach numbers of 1.55, 2.00, 2.50, 3.00, and 3.50 at a Reynolds number of 1.5 million based on the mean aerodynamic chord. Consideration of these data leads to the following general conclusions:

1. The complete model was statically stable both longitudinally and directionally at all test Mach numbers. However, the effective dihedral was negative $\left(+C_{l_\beta}\right)$ at a Mach number of 1.55 and at negative angles of attack but at all other test conditions it was positive or near zero.

2. In general, the addition of speed brakes provided increased damping in yaw and directional stability with little effect on the longitudinal derivatives; however, with increasing angle of attack above Mach numbers of 2.5, the effective dihedral was decreased.

3. A modification of the vertical tail from an 11.5° double-wedge section to a 10° single-wedge section of 5 percent less area provided an appreciable increase in directional stability and damping in yaw at Mach numbers of 2.5, 3.0, and 3.5.

Ames Research Center
National Aeronautics and Space Administration
Moffett Field, Calif., Sept. 8, 1958

REFERENCES

1. Beam, Benjamin H., and Endicott, Kenneth C.: Wind-Tunnel Data on the Longitudinal and Lateral-Directional Rotary Derivatives of a Straight-Wing, Research Airplane Configuration at Mach Numbers From 2.5 to 3.5. NACA RM A58A14, 1958.

2. Huntsberger, Ralph F., Jr., and Parsons, John F.: The Design of Large High-Speed Wind Tunnels. NACA Paper Presented at Fourth General Assembly of the AGARD Wind Tunnel Panel, Scheveningen, The Netherlands, AG15/P6, May 3-7, 1954.

3. Beam, Benjamin H.: A Wind-Tunnel Test Technique for Measuring the Dynamic Rotary Stability Derivatives at Subsonic and Supersonic Speeds. NACA Rep. 1258, 1956. (Supersedes NACA TN 3347)

4. Lopez, Armando E., and Tinling, Bruce E.: The Static and Dynamic-Rotary Stability Derivatives at Subsonic Speeds of a Model of the X-15 Research Airplane. NACA RM A58F09, 1958.

5. Chapman, Dean R., and Kester, Robert H.: Effect of Trailing-Edge Thickness on Lift at Supersonic Velocities. NACA TN 3504, 1955. (Supersedes NACA RM A52D17)

[redacted]

TABLE I.- GEOMETRIC CHARACTERISTICS OF MODEL

Wing (leading and trailing edges extended to body center line)	
Aspect ratio	2.500
Taper ratio	0.200
Root chord, ft	1.342
Tip chord, ft	0.268
Leading-edge sweep angle, deg	36.75
Dihedral angle, deg	0
Incidence angle, deg	0
Twist, deg	0
Airfoil section	NACA 66 series (modified)
Thickness ratio	0.0445
Area, sq ft	1.620
Span, ft	2.010
Mean aerodynamic chord, ft	0.924
Horizontal tail (leading and trailing edges extended to body center line and projected to wing chord plane)	
Aspect ratio	2.92
Taper ratio	0.206
Sweepback of quarter chord, deg	45
Dihedral angle, deg	-15
Twist, deg	0
Airfoil section	NACA 66 series (modified)
Thickness ratio	0.0500
Area, sq ft	0.903
Span, ft	1.620
Root chord, ft	0.920
Tip chord, ft	0.190
Mean aerodynamic chord, ft	0.635
Length 0.25 $\bar{c}_w$ to 0.50 $\bar{c}_h$, ft	1.221
Upper vertical tail (leading and trailing edges extended to wing chord plane)	
Taper ratio	0.656
Leading-edge sweep angle, deg	30
Airfoil section, single wedge, deg	10
Root chord, ft	1.039
Tip chord, ft	0.681
Area, sq ft	0.535
Span, ft	0.622
Mean aerodynamic chord, ft	0.870
Length 0.25 $\bar{c}_w$ to 0.50 $\bar{c}_v$, ft	1.252
Height, $\bar{c}$ to fuselage reference line, ft	0.290

[redacted]

TABLE I.- GEOMETRIC CHARACTERISTICS OF MODEL - Concluded

Lower vertical tail (leading and trailing edges extended to wing chord plane)		
Taper ratio		0.693
Leading-edge sweep angle, deg		30
Airfoil section, single wedge, deg		10
Root chord, ft		1.039
Tip chord, ft		0.720
Area, sq ft		0.481
Span, ft		0.547
Mean aerodynamic chord, ft		0.886
Length 0.25 $\bar{c}_w$ to 0.50 $\bar{c}_v$, ft		1.245
Height, $\bar{c}$ to fuselage reference line, ft		0.258
Fuselage	Without side fairings	With side fairings
Length, ft	4.425	4.425
Base area, sq ft	0.101	0.161
Frontal area, sq ft	0.139	0.173
Moment reference (on fuselage center line)		
Longitudinal location (0.25 $\bar{c}_w$)		
Aft of nose, ft		2.618

[redacted]

[redacted]

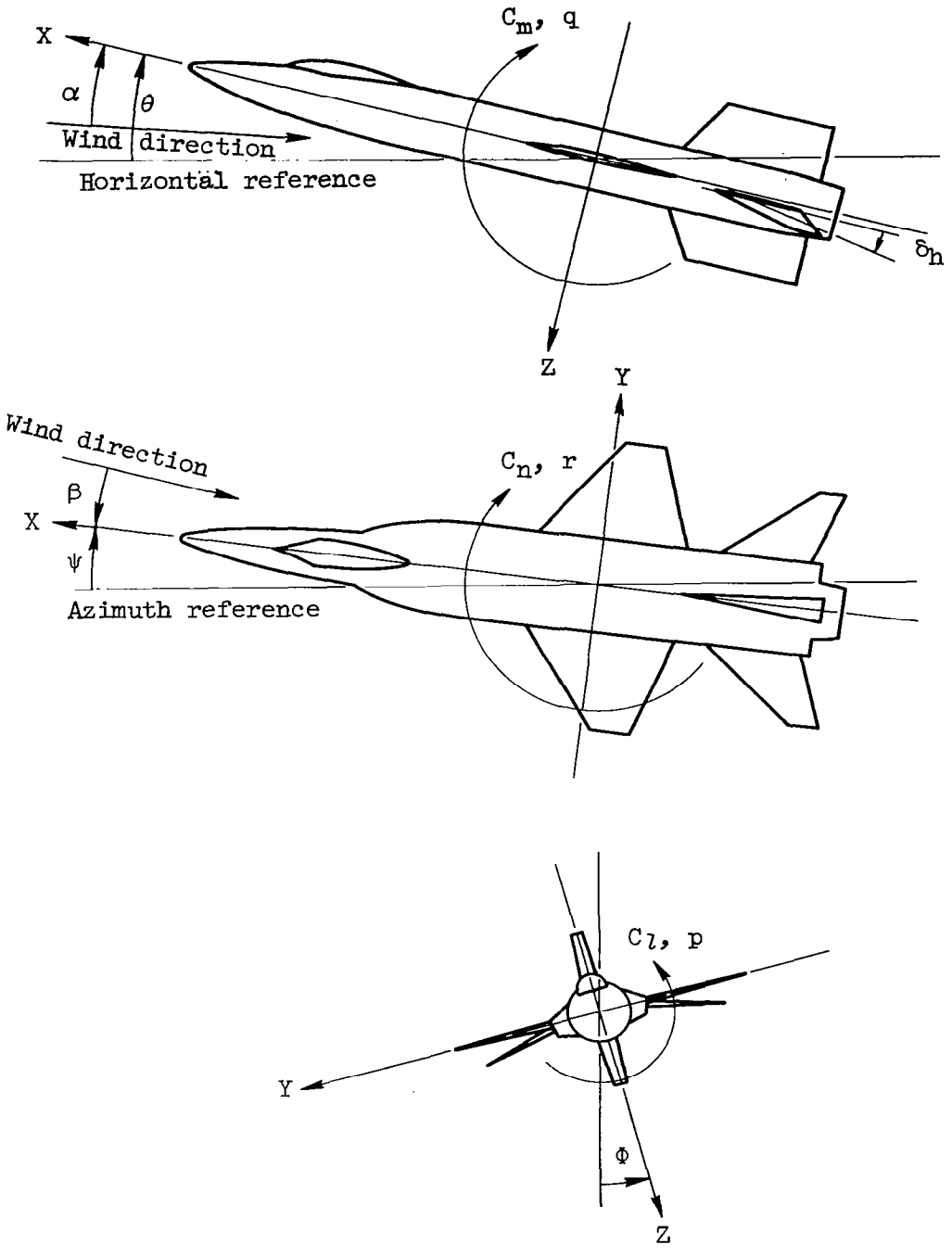

Figure 1.- The body system of axes. Arrows indicate positive directions of moments and angles.

Note: All dimensions are in feet

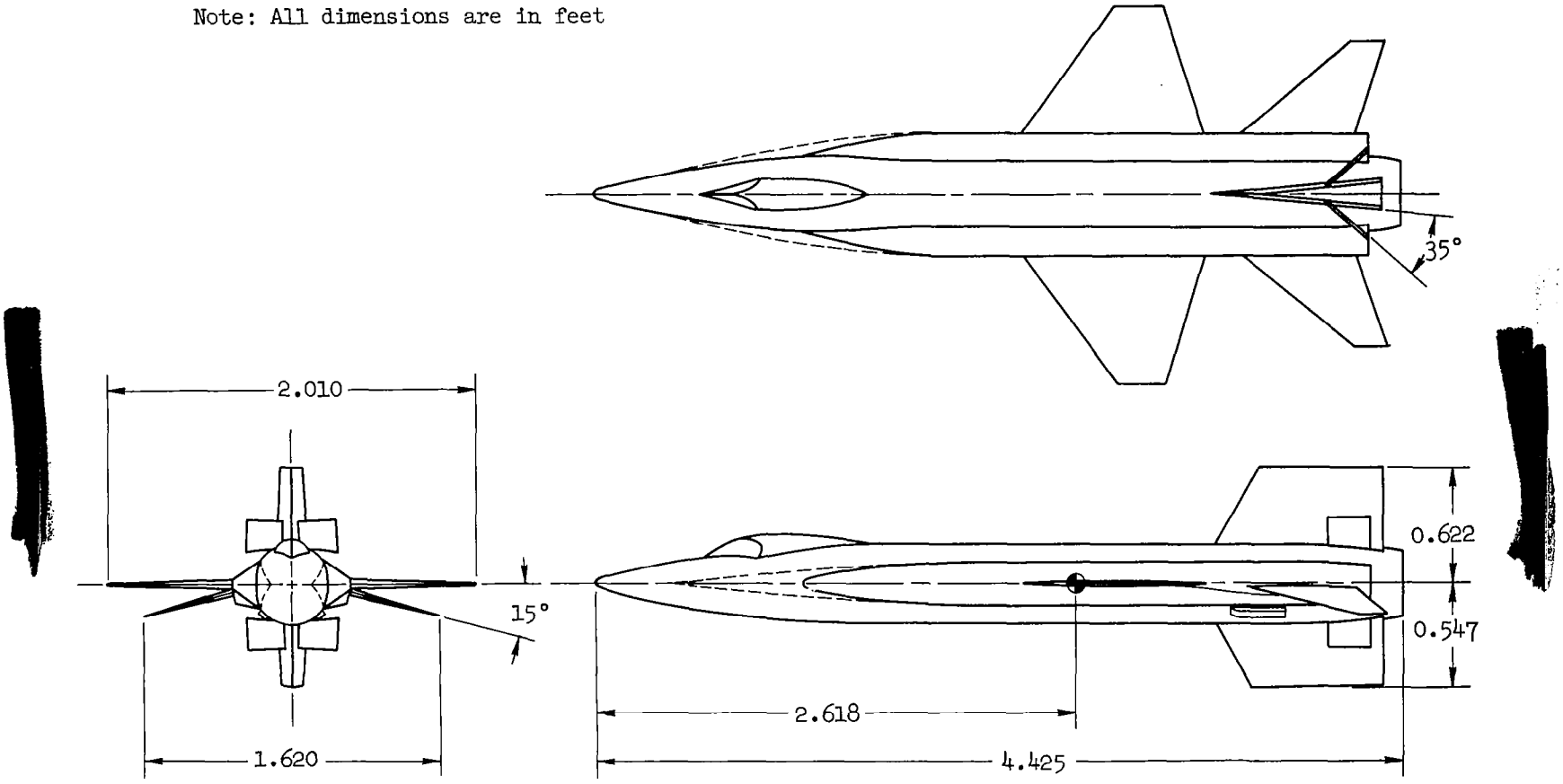

Figure 2.- Sketch of the X-15 research airplane model showing some of the important dimensions.

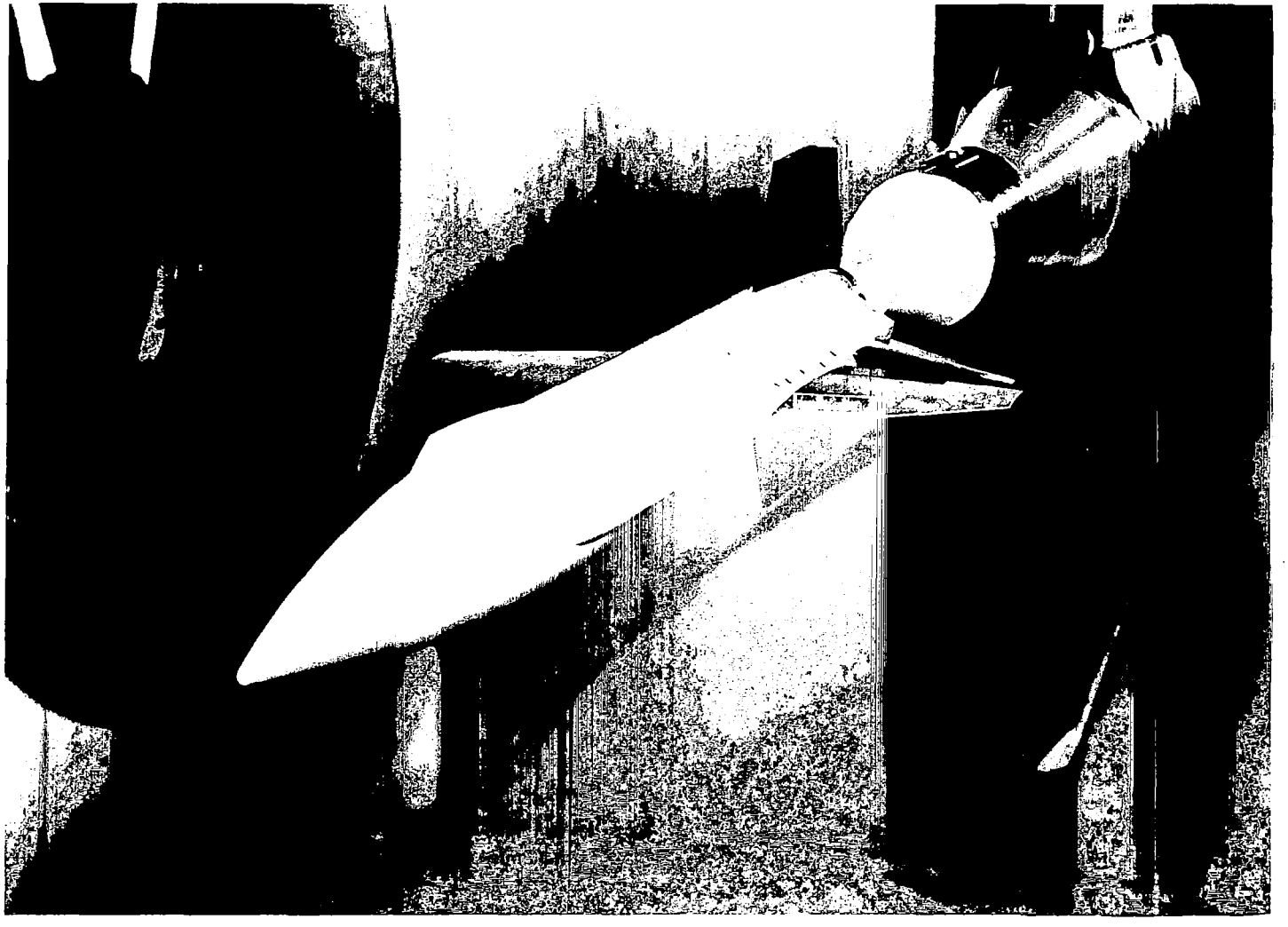

A-22585

(a) 8- by 7-foot test section.

Figure 3.- The X-15 model mounted in the Unitary Plan wind tunnel.

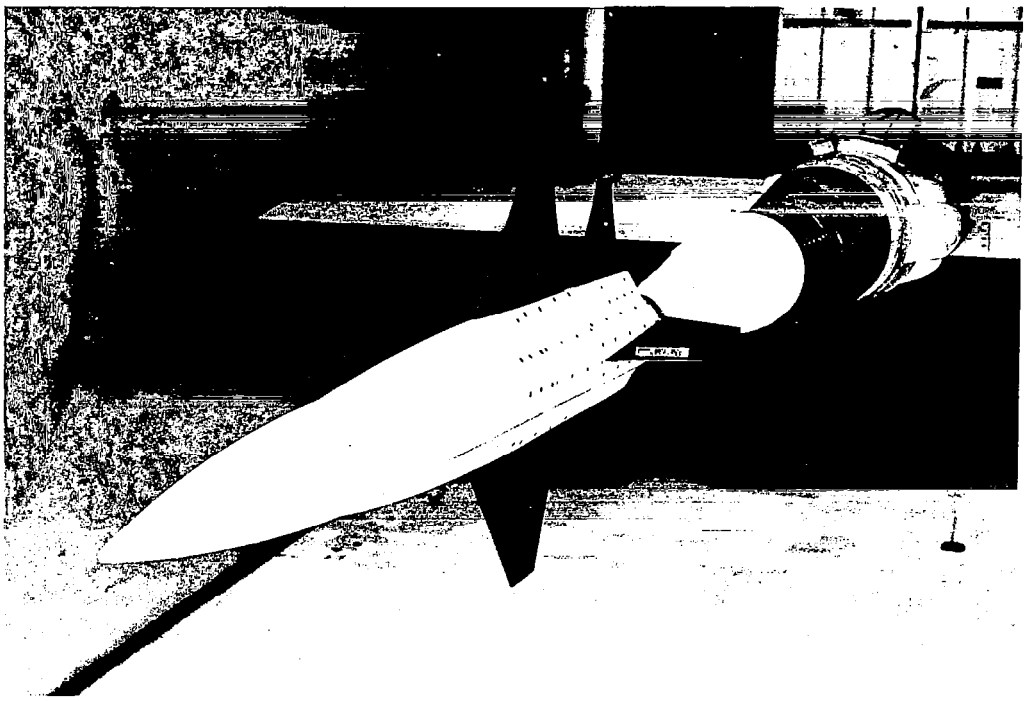

A-22750

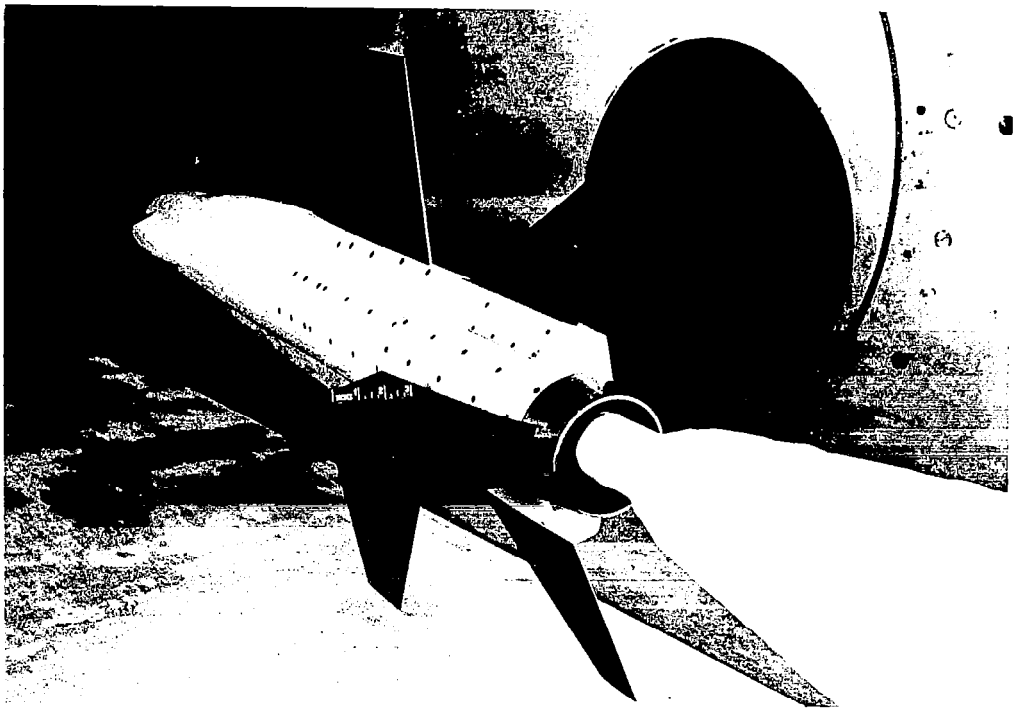

A-22751

(b) 9- by 7-foot test section.

Figure 3.- Concluded.

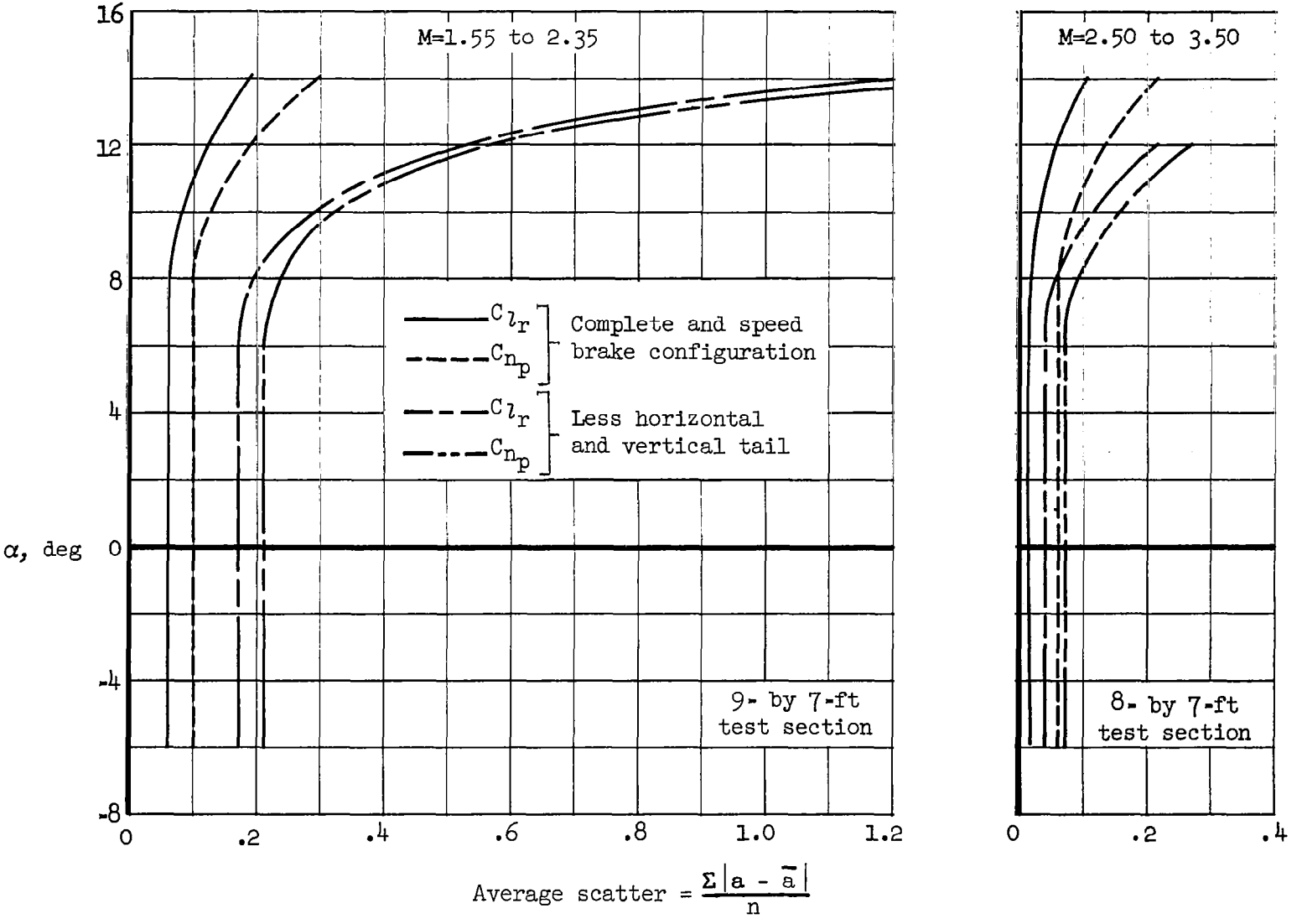

Figure 4.- Average scatter in three to eight data points as a function of angle of attack for the cross-derivative data.

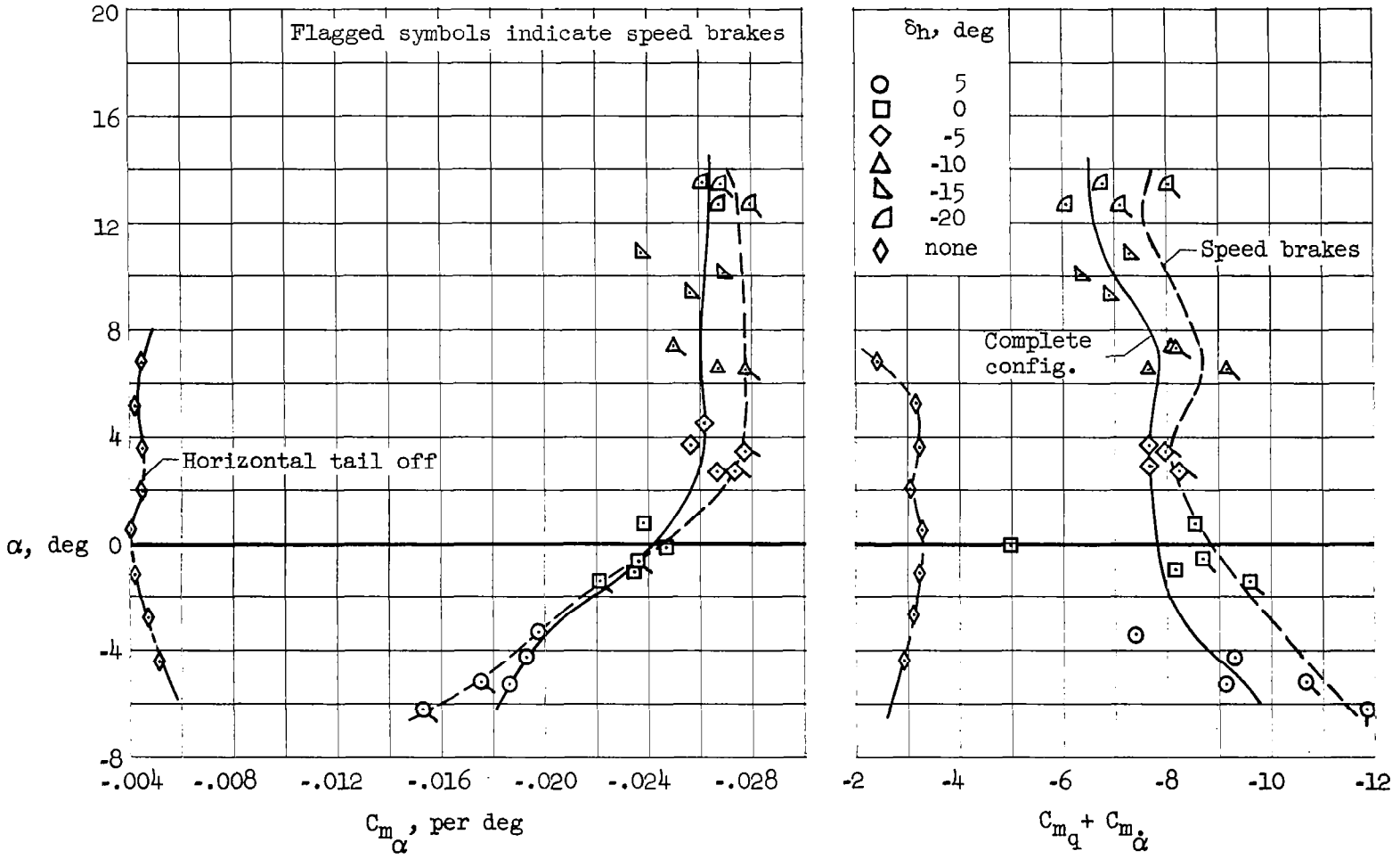

(a) M = 1.55

Figure 5.- The variation of the static longitudinal stability and damping in pitch with angle of attack.

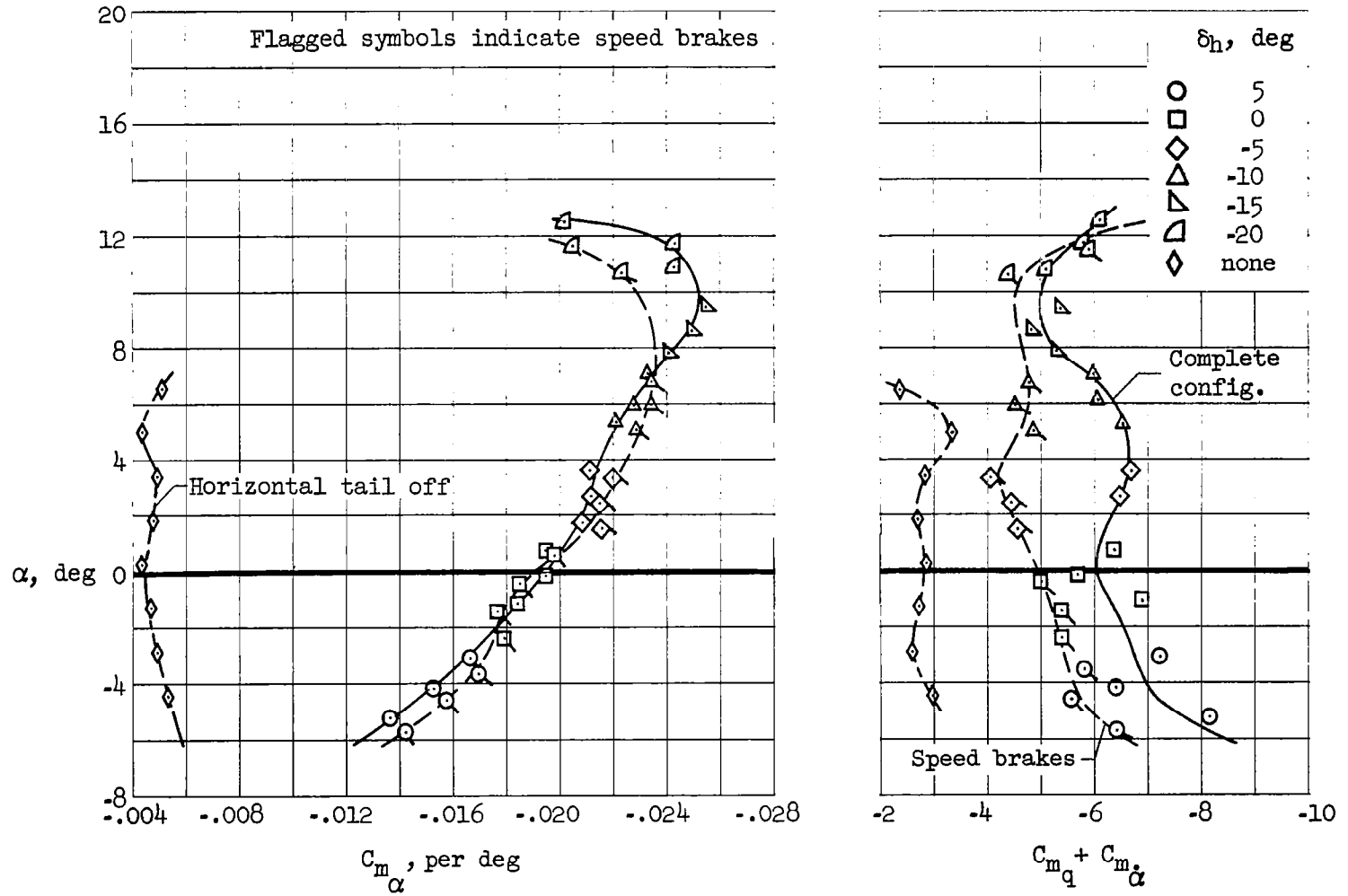

(b) M = 2.00

Figure 5.- Continued.

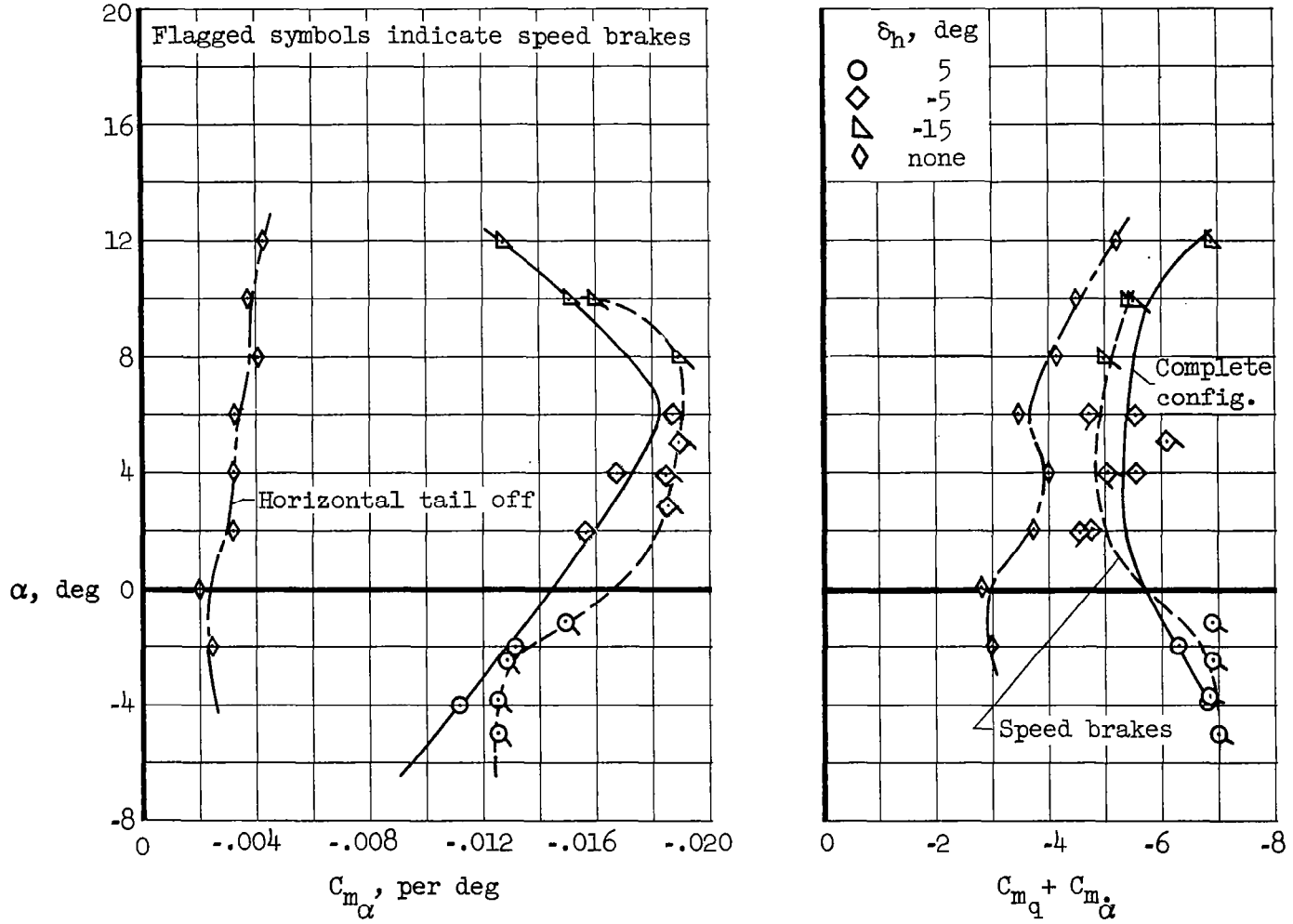

(c) M = 2.50

Figure 5.- Continued.

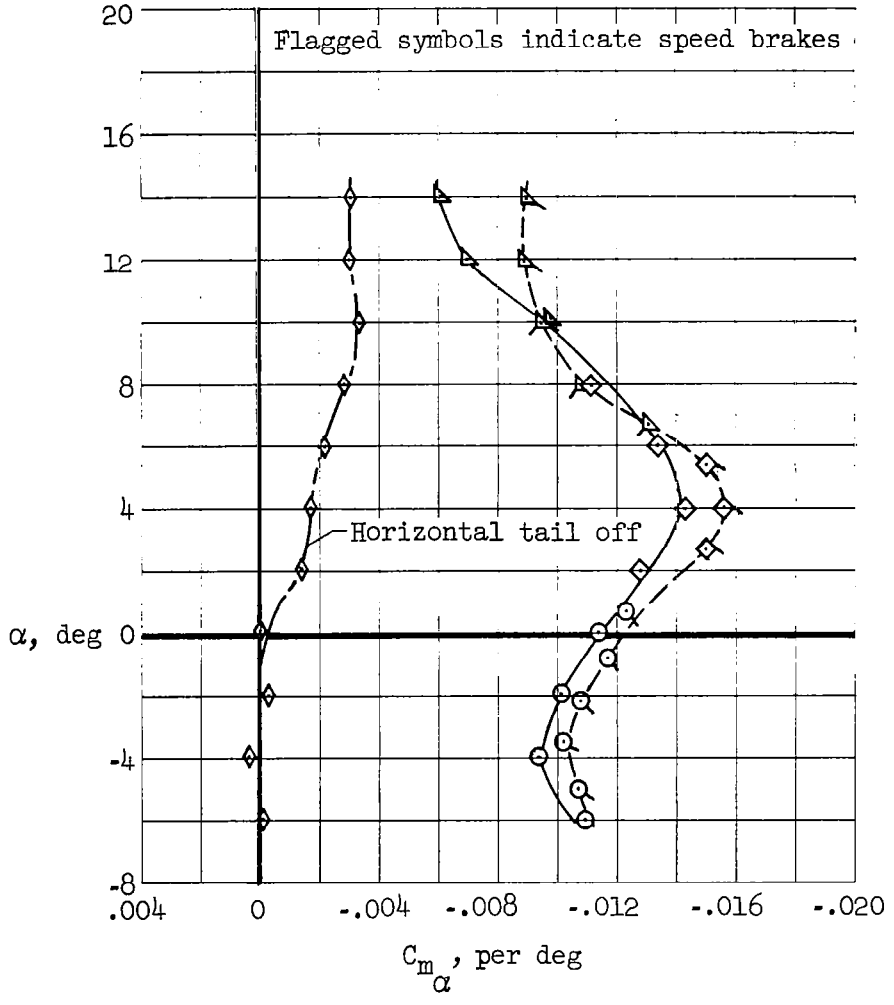

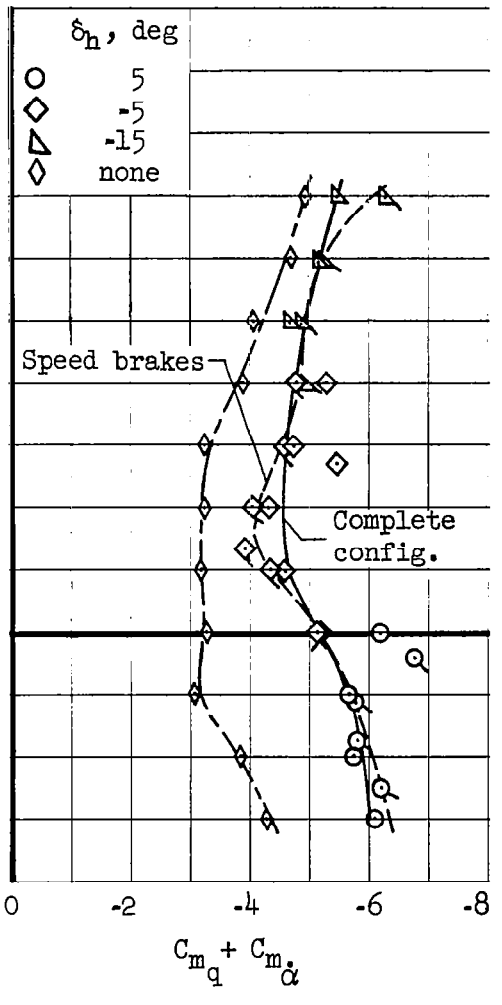

(d) M = 3.00

Figure 5.- Continued.

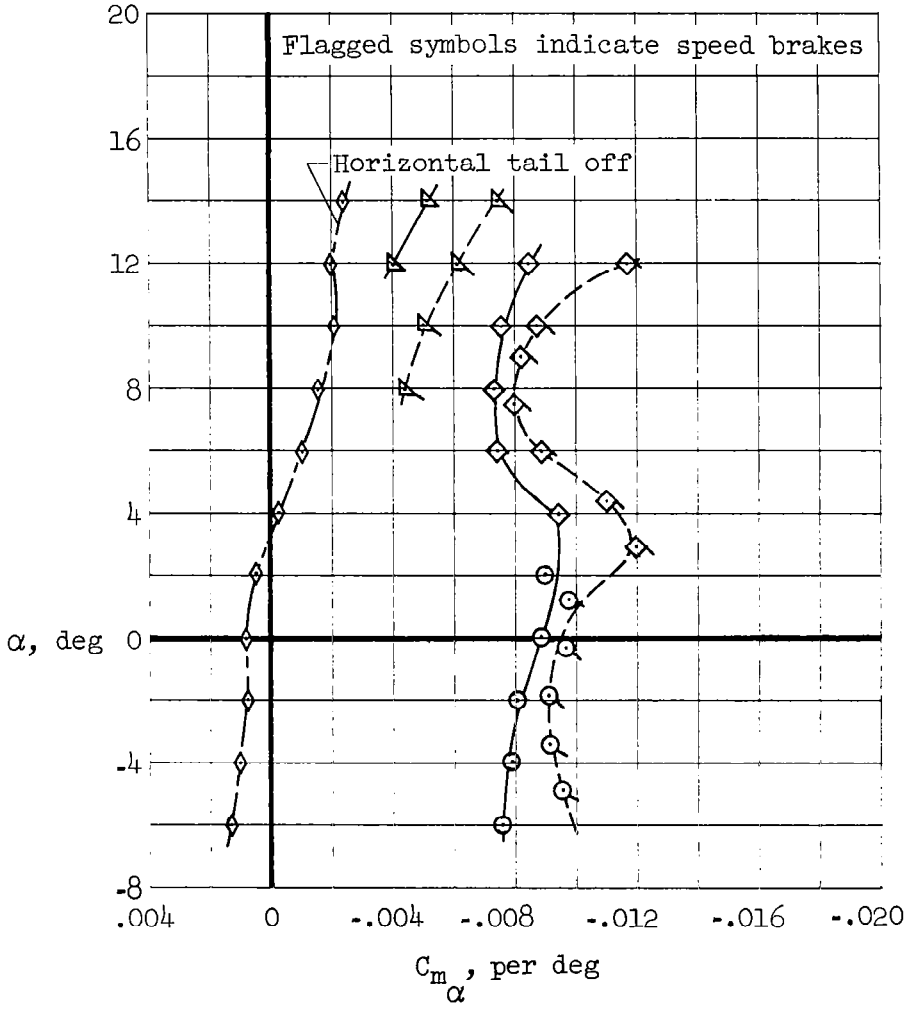

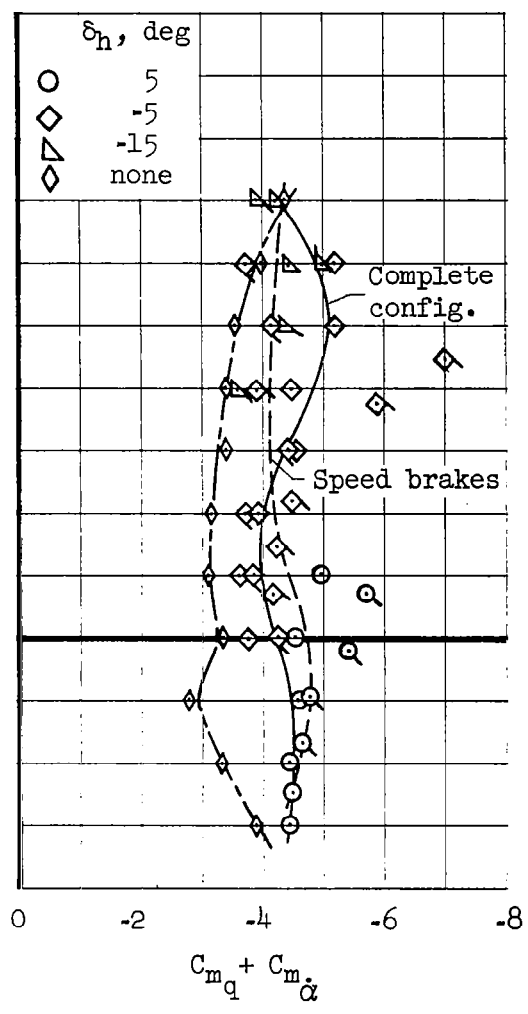

(e) M = 3.50

Figure 5.- Concluded.

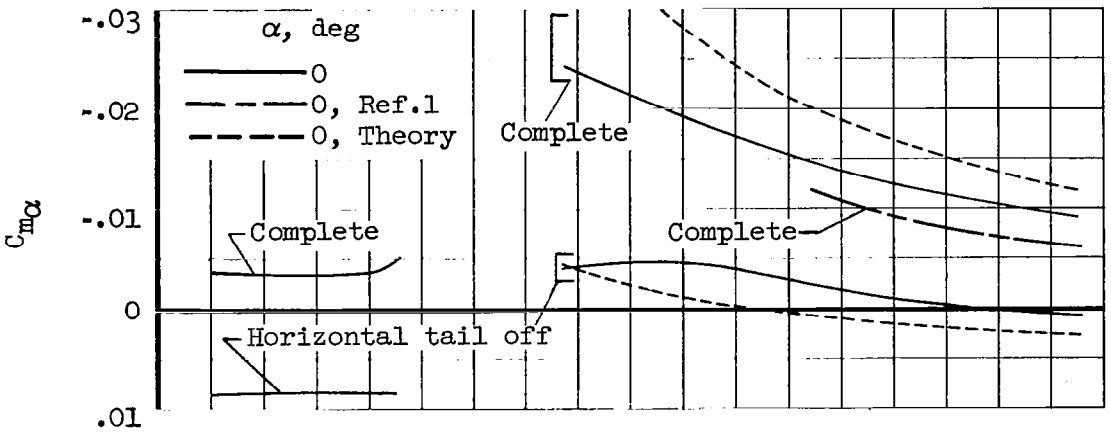

(a) Complete configuration and horizontal tail off.

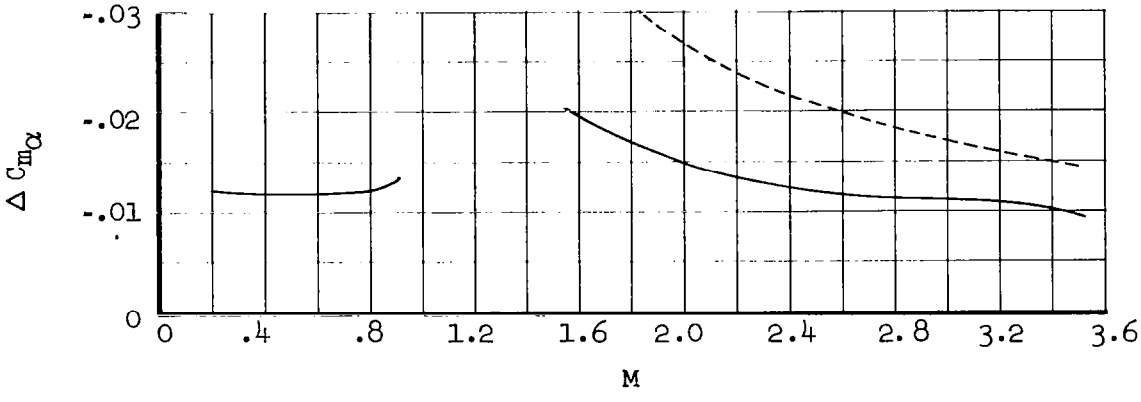

(b) Horizontal-tail contribution.

Figure 6.- The variation with Mach number of the static longitudinal stability derivative for the complete configuration both with and without the horizontal tail.

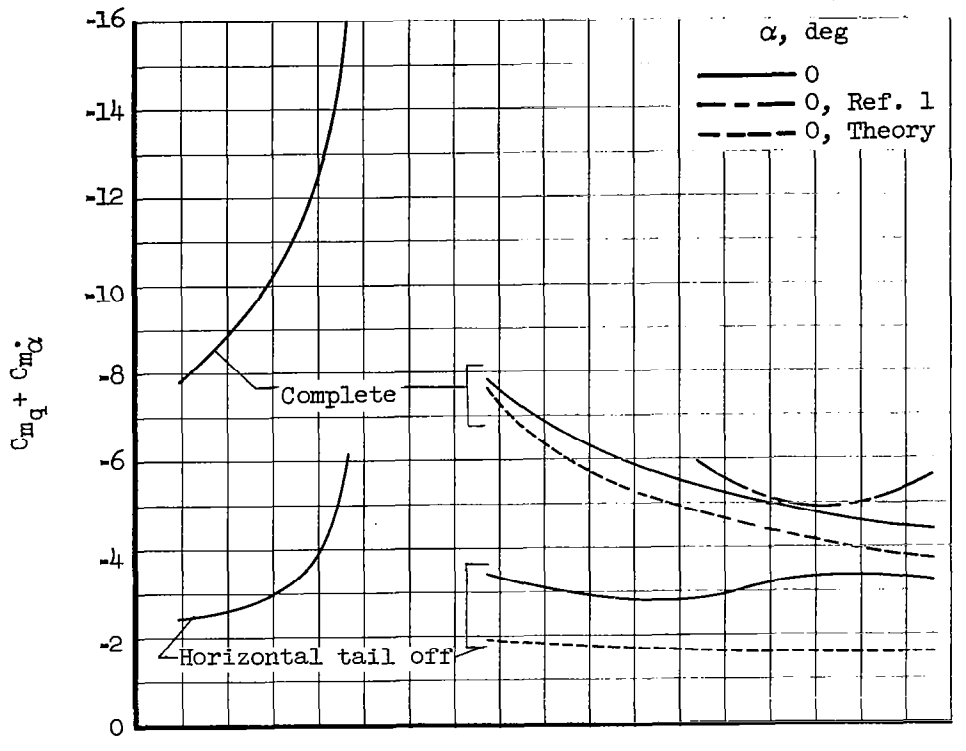

(a) Complete configuration and horizontal tail off.

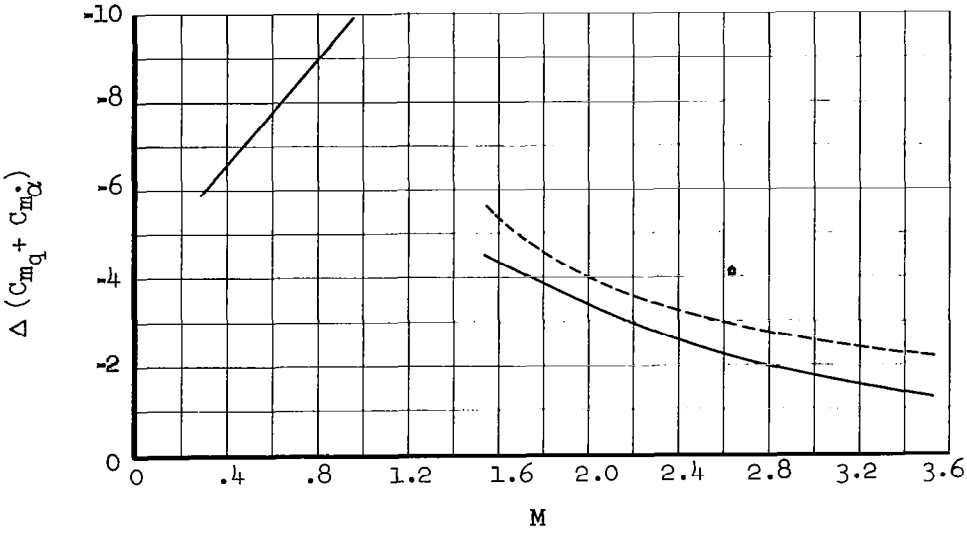

(b) Horizontal-tail contribution.

Figure 7.- The variation with Mach number of the damping in pitch for the complete configuration both with and without the horizontal tail.

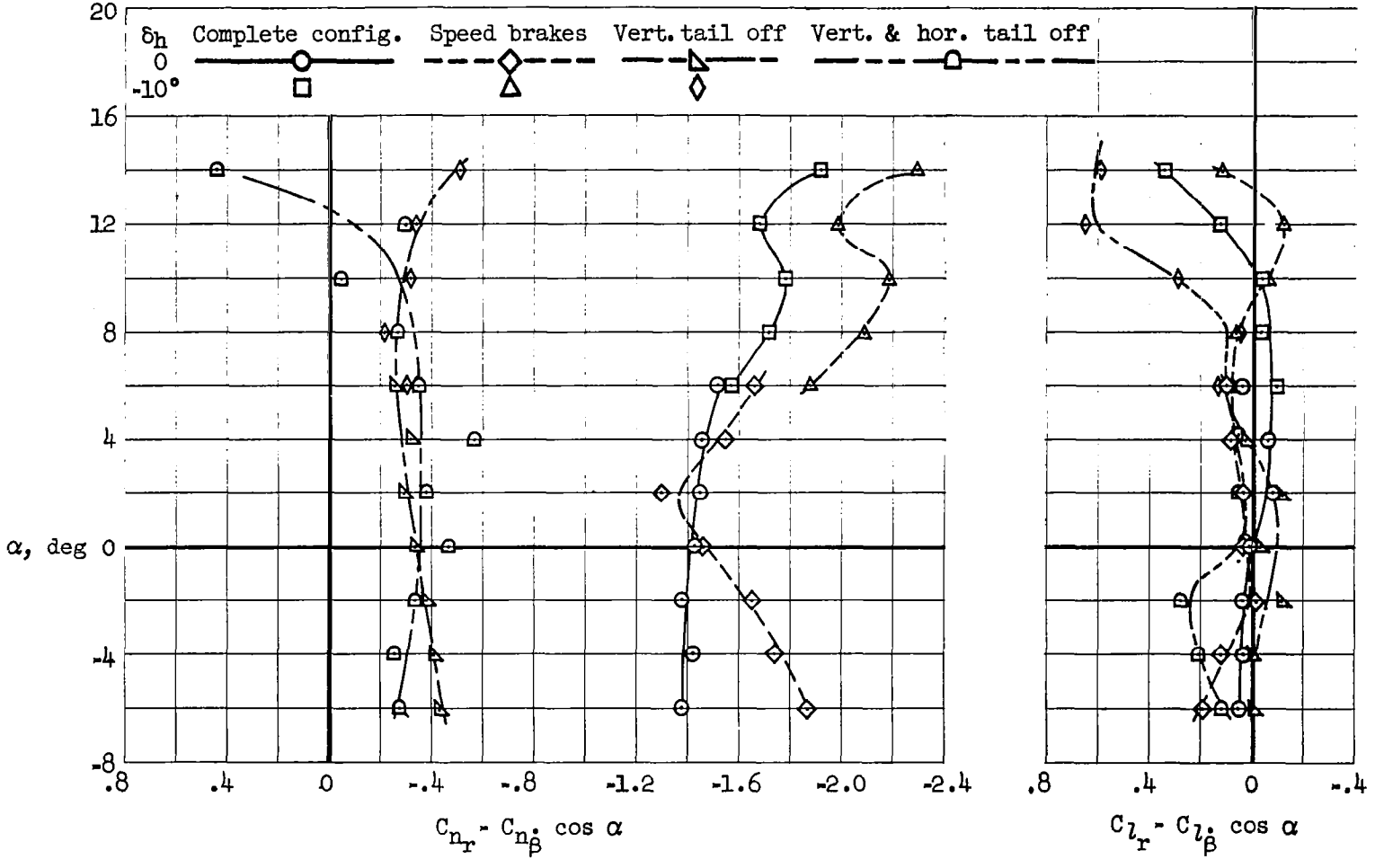

(a) M = 1.55

Figure 8.- The variation of damping in yaw and rolling moment due to yawing with angle of attack.

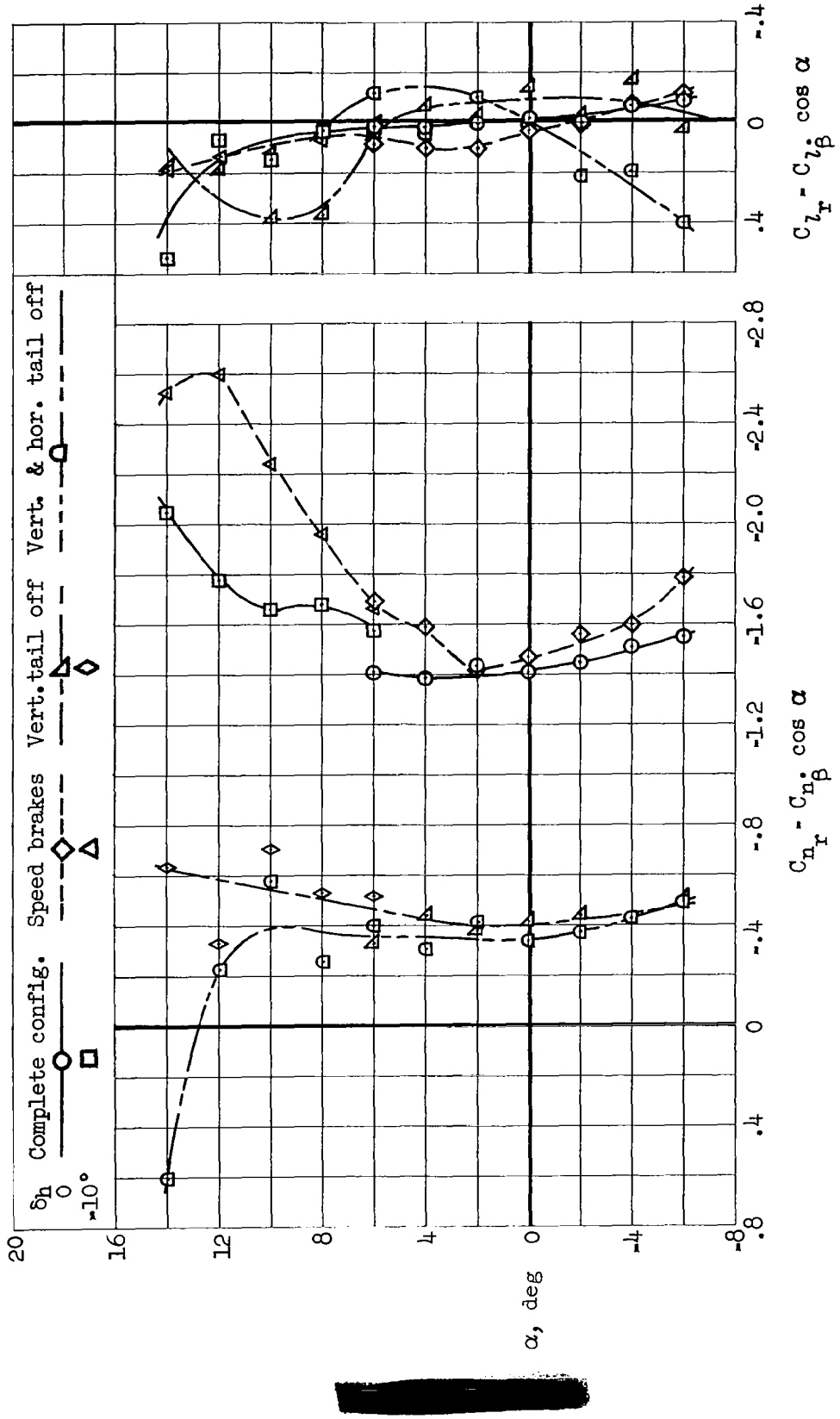

(b) M = 2.00

Figure 8.- Continued.

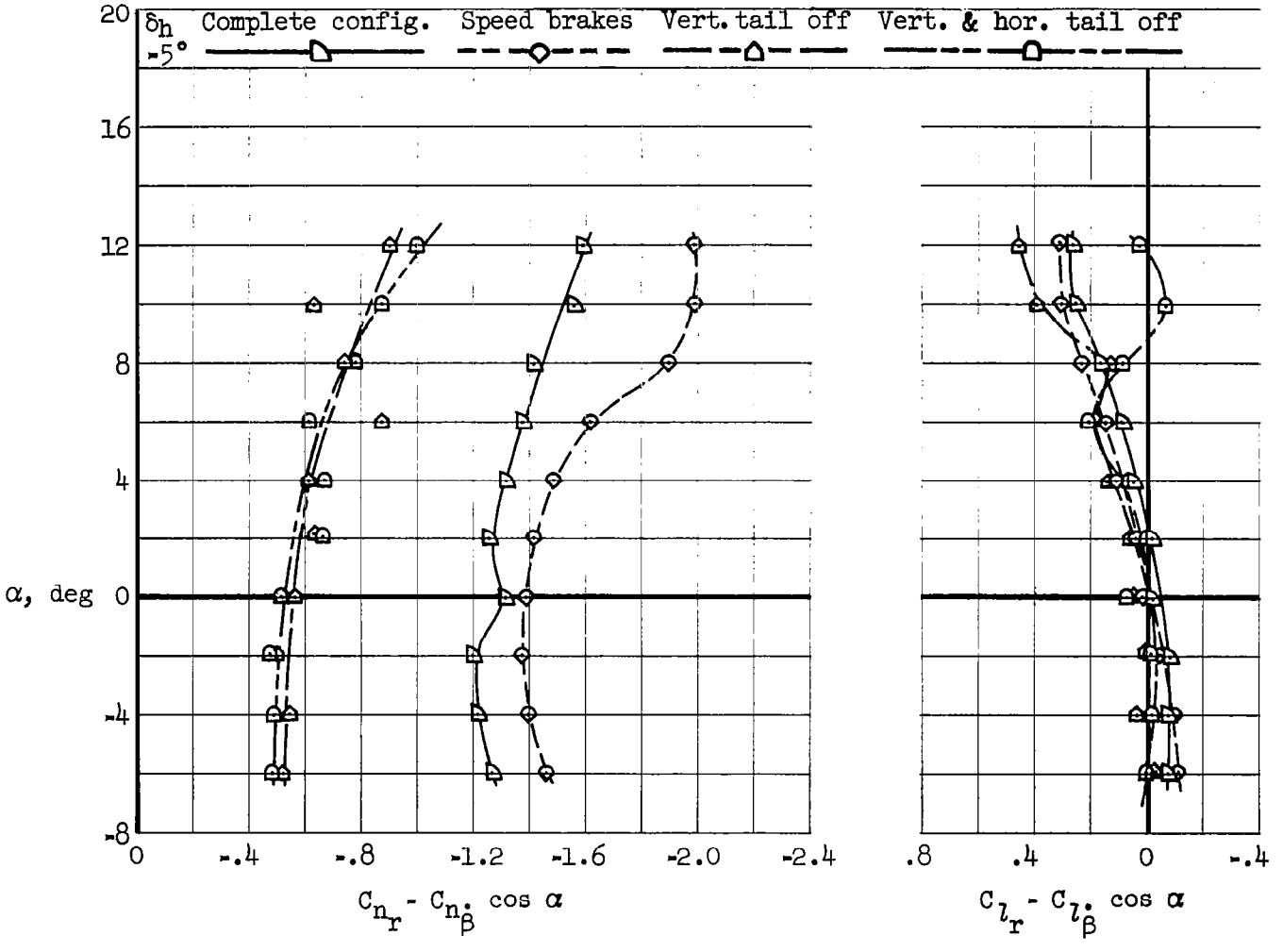

(c) M = 2.50

Figure 8.- Continued.

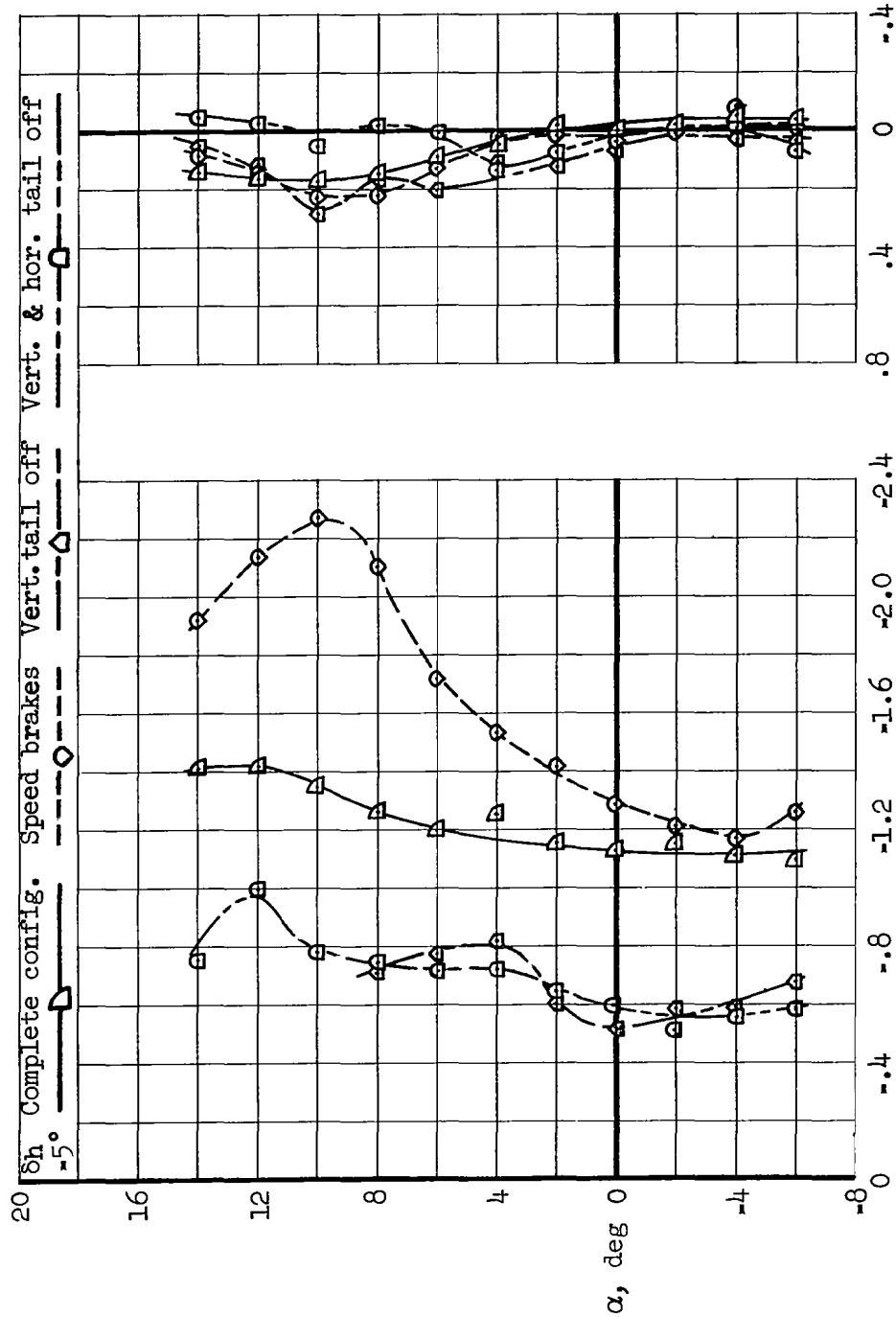

(d) M = 3.00

Figure 8.- Continued.

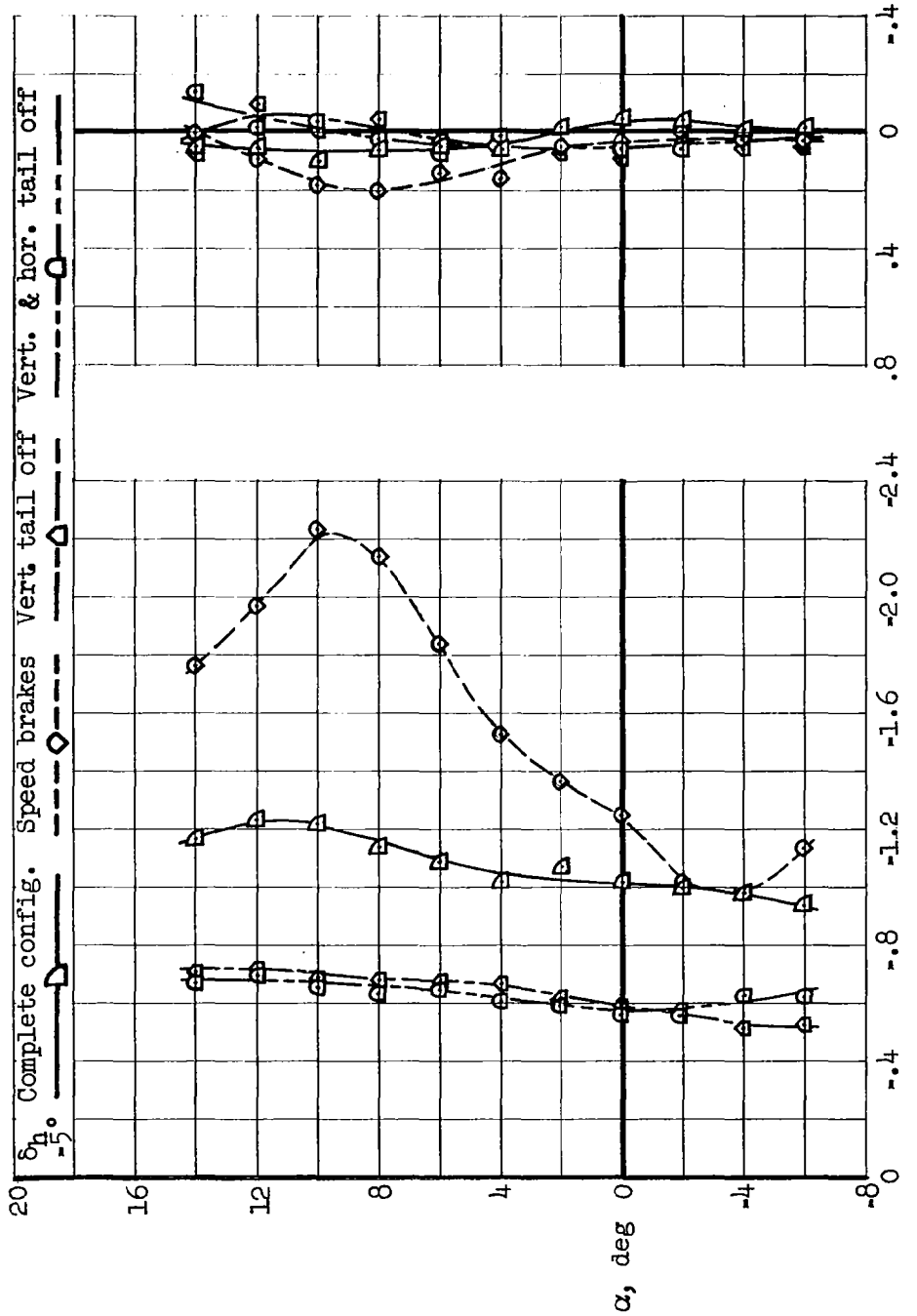

(e) M = 3.50

Figure 8.- Concluded.

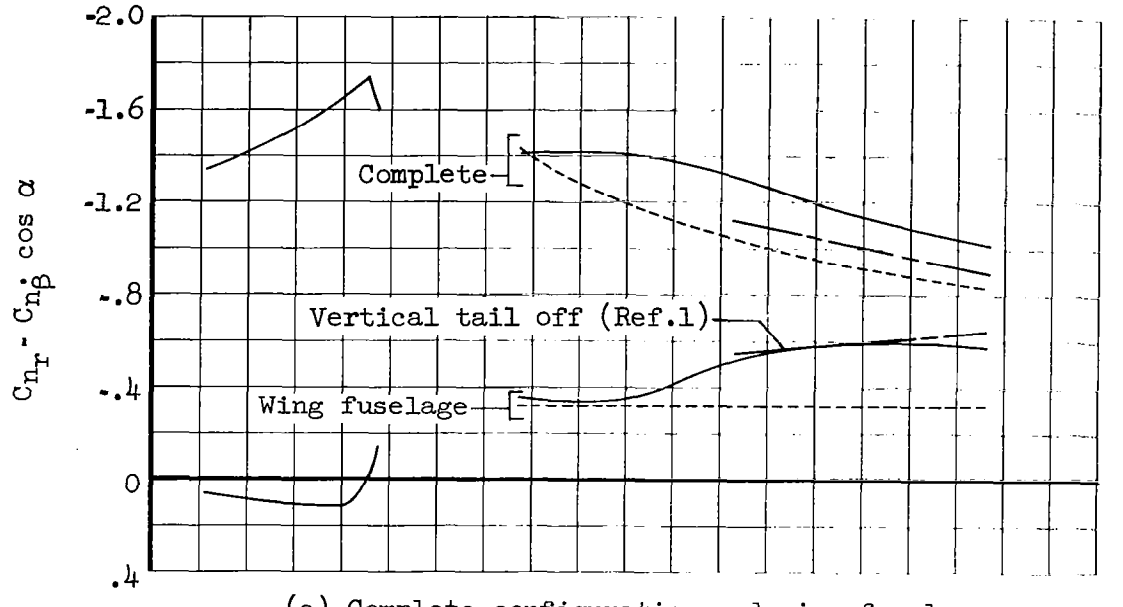

(a) Complete configuration and wing fuselage.

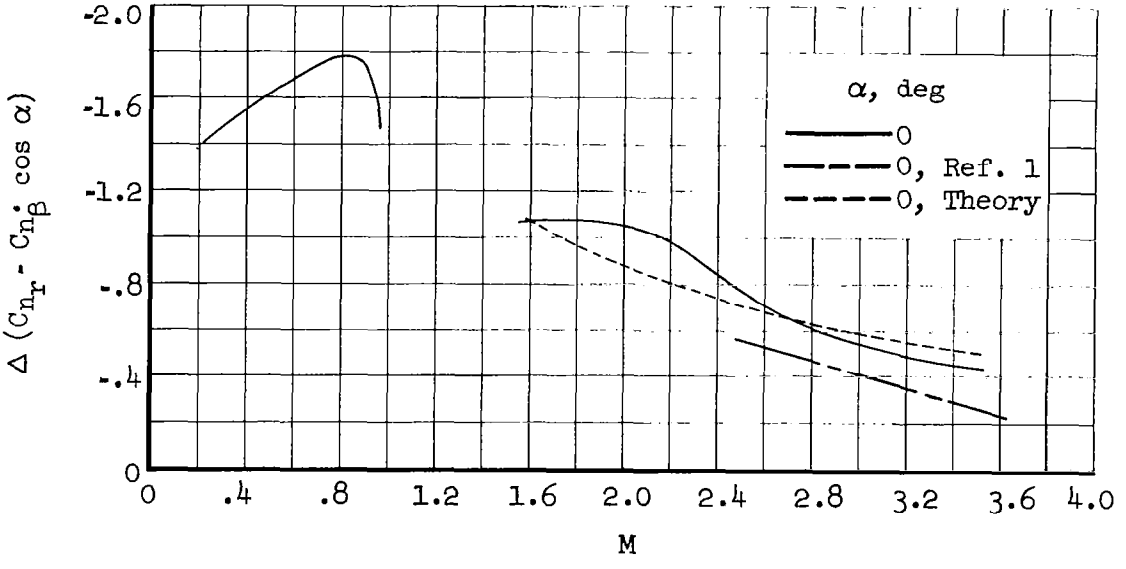

(b) Vertical-tail contribution.

Figure 9.- The variation with Mach number of the damping in yaw for the complete configuration both with and without the vertical and horizontal tail.

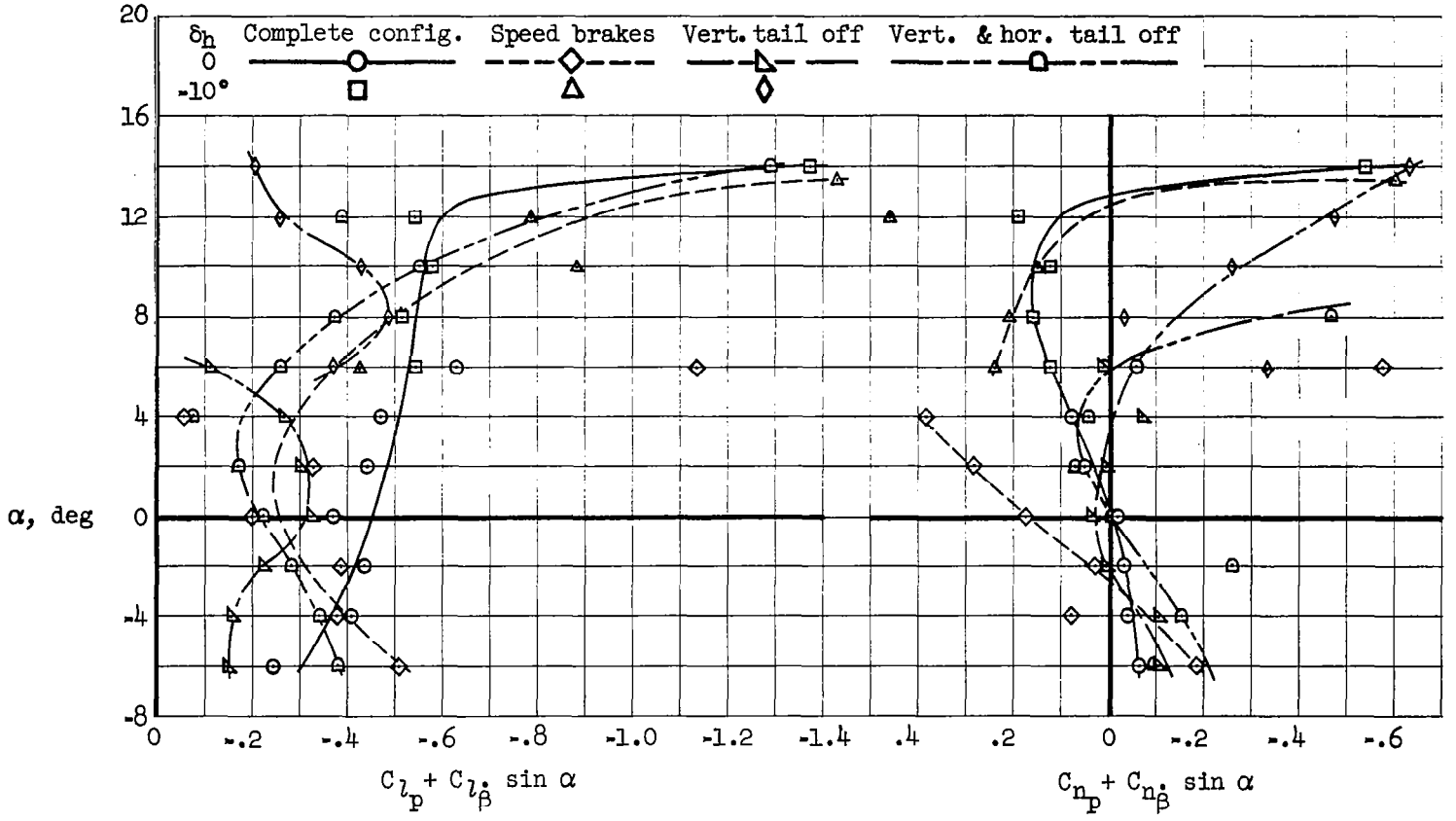

(a) M = 1.55

Figure 10.- The variation of damping in roll and yawing moment due to rolling with angle of attack.

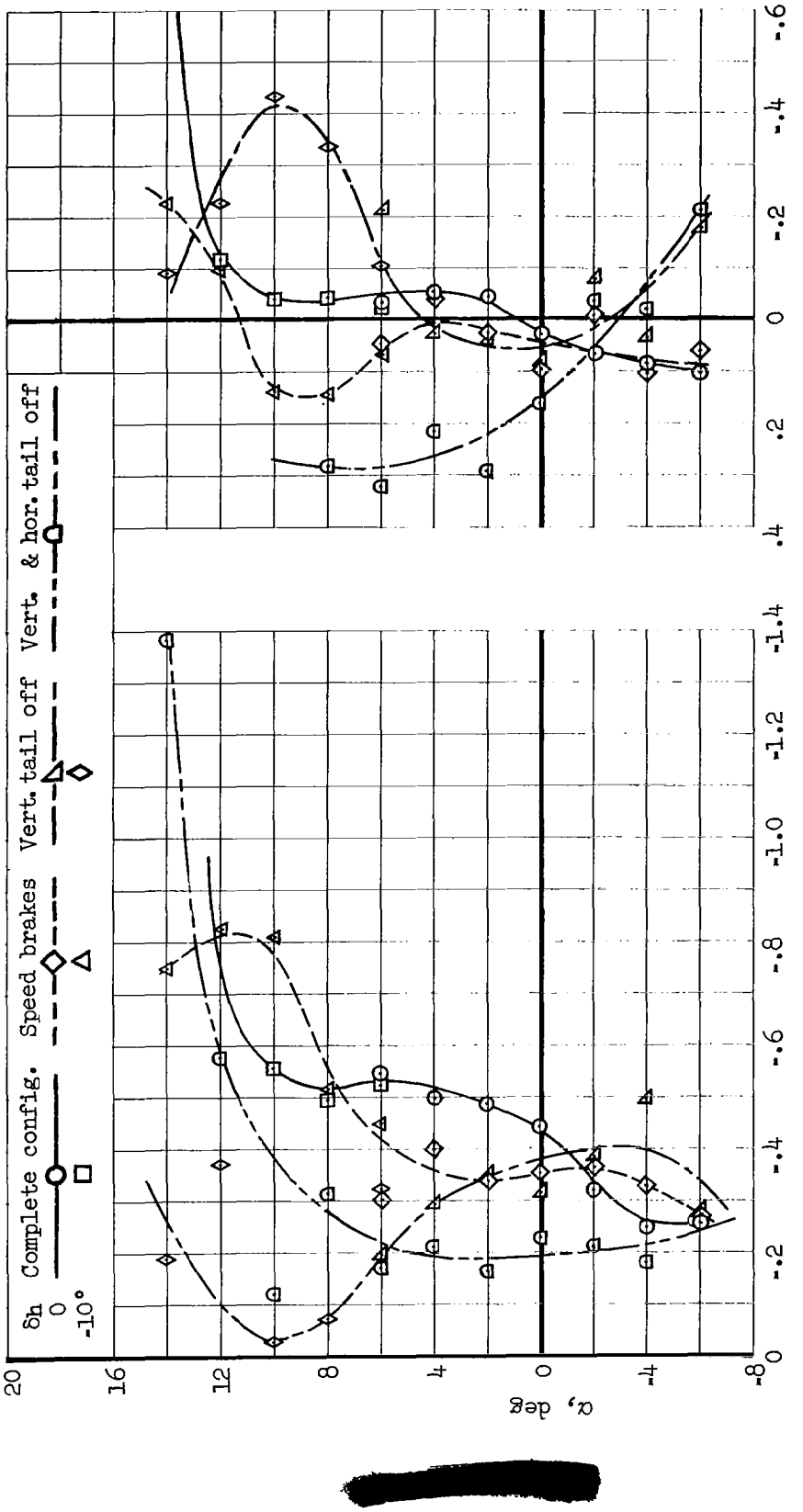

(b) M = 2.00

Figure 10.- Continued.

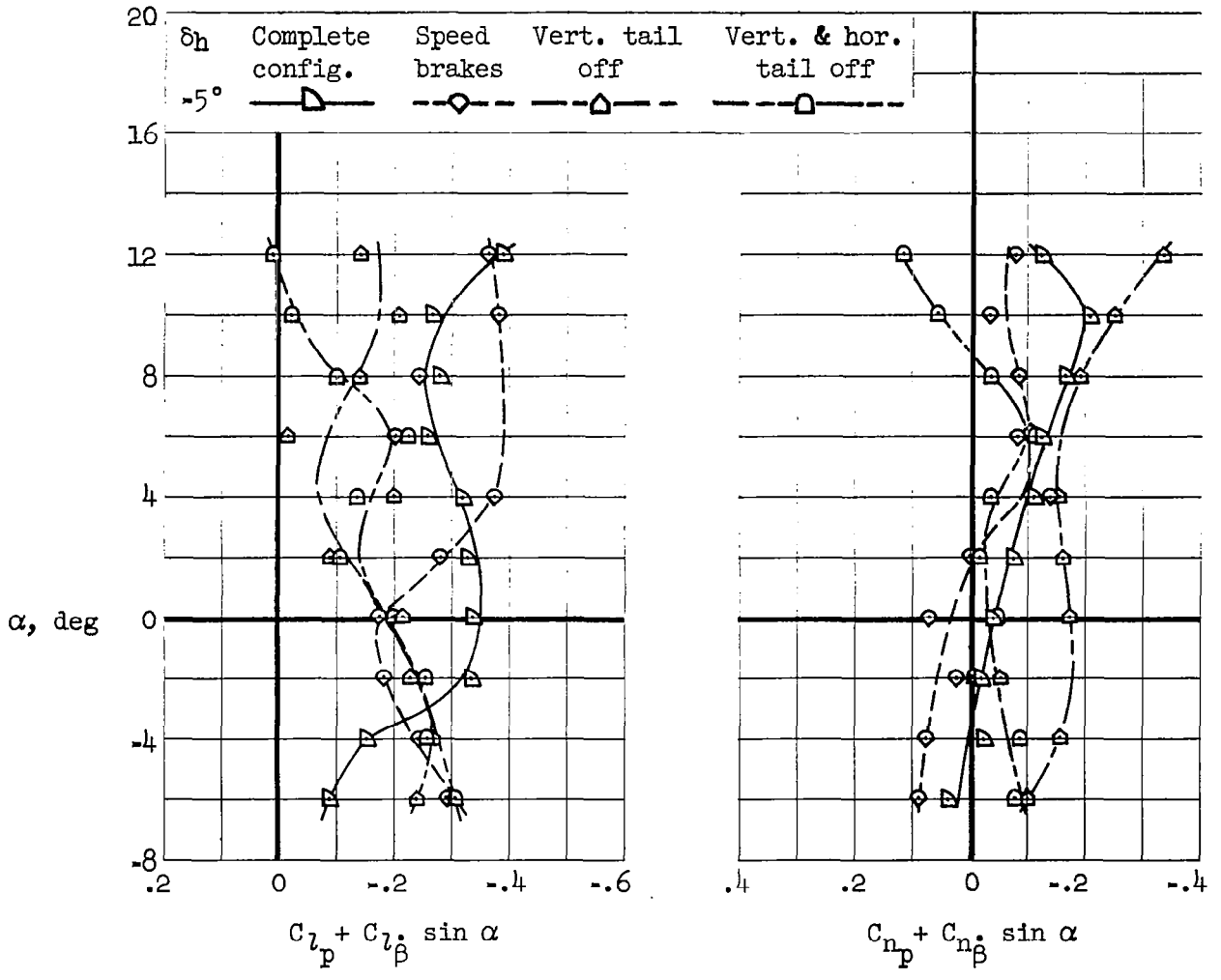

(c) M = 2.50

Figure 10.- Continued.

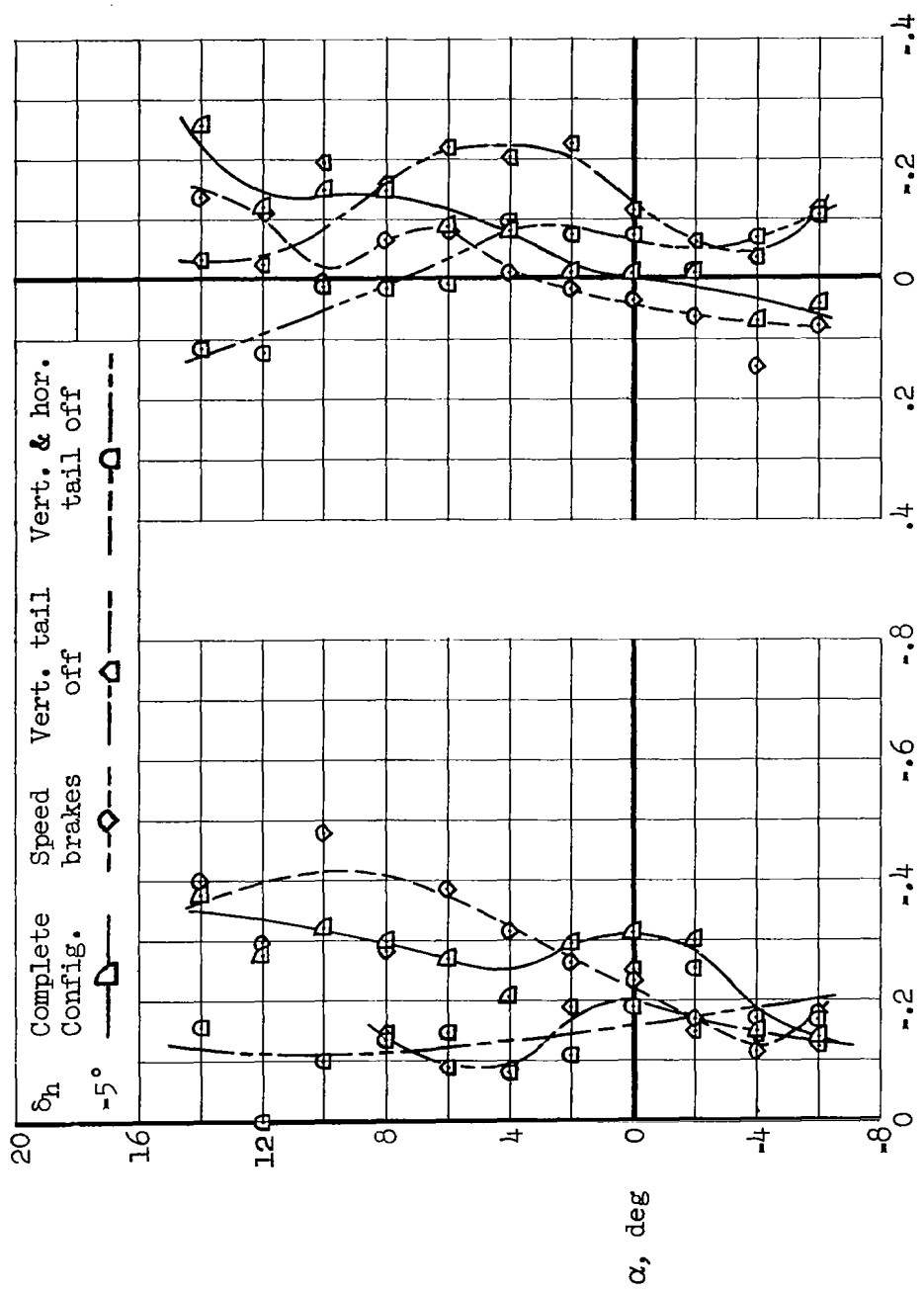

(d) M = 3.00

Figure 10.- Continued.

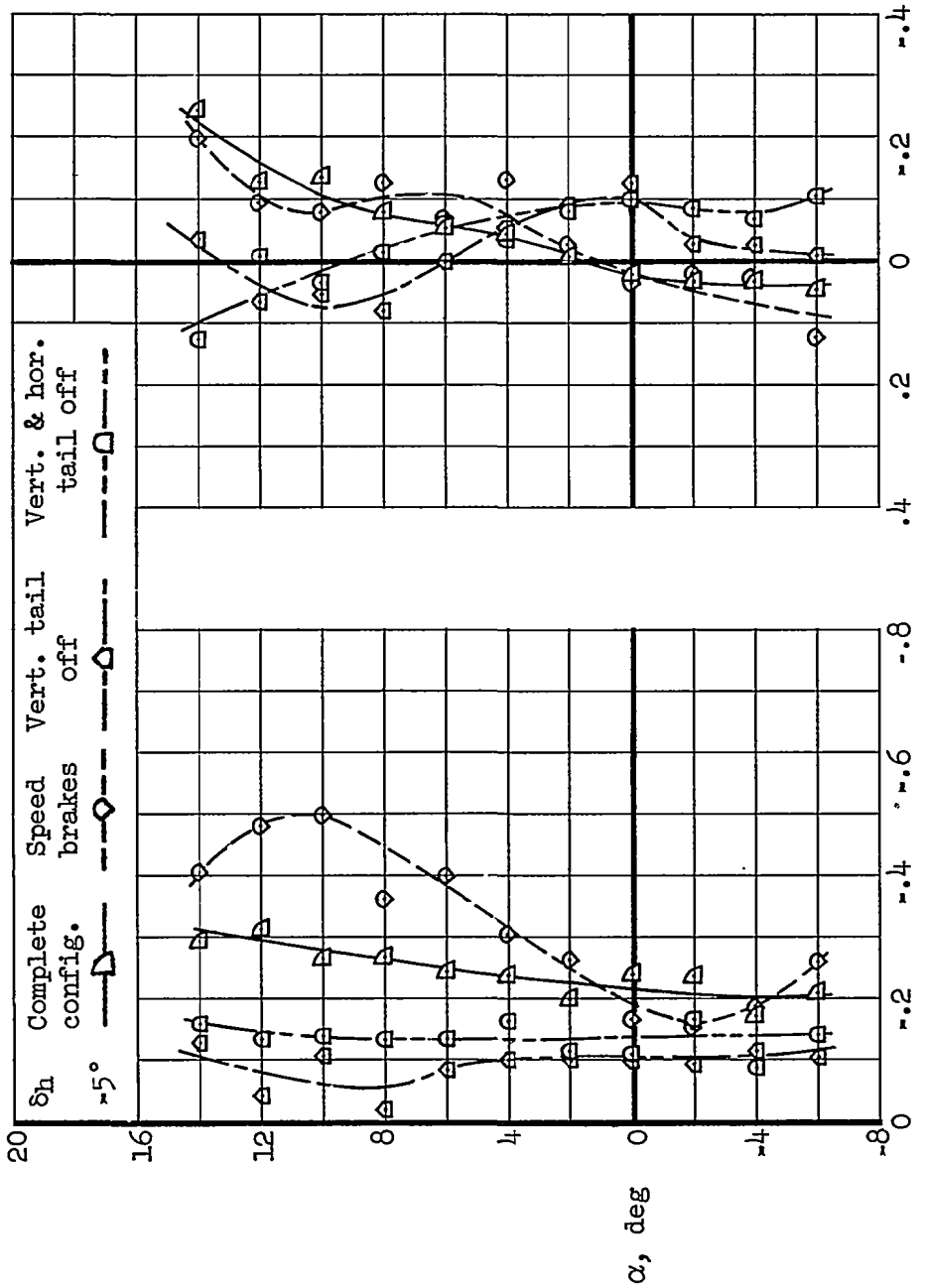

(e) M = 3.50

Figure 10.- Concluded.

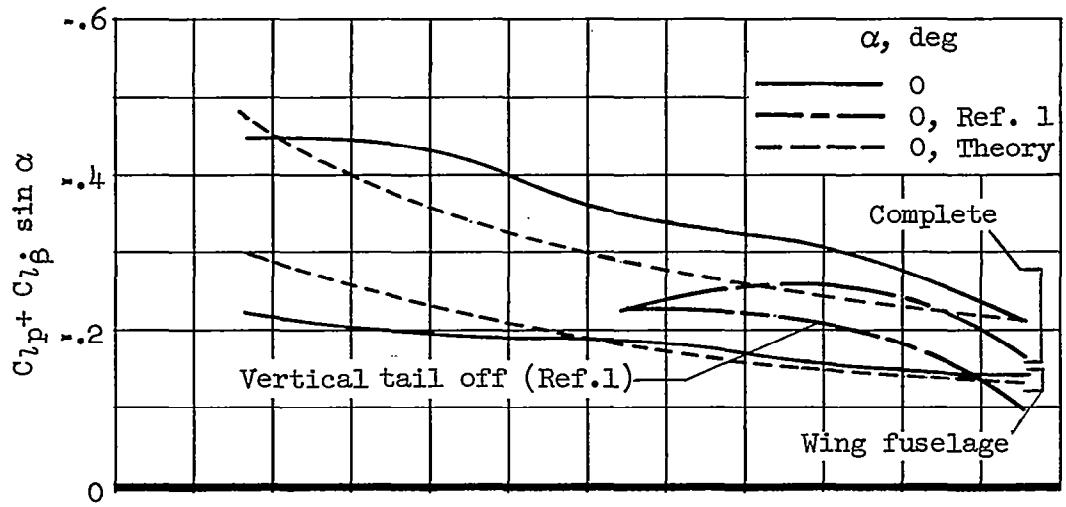

(a) Complete configuration and wing fuselage.

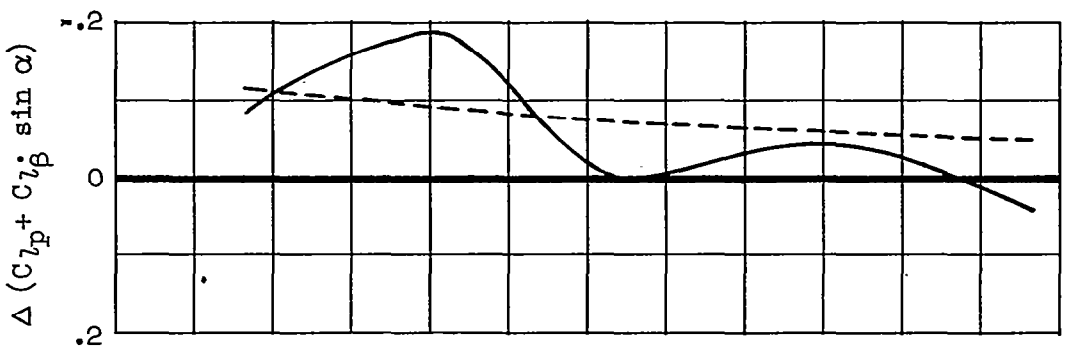

(b) Horizontal-tail contribution.

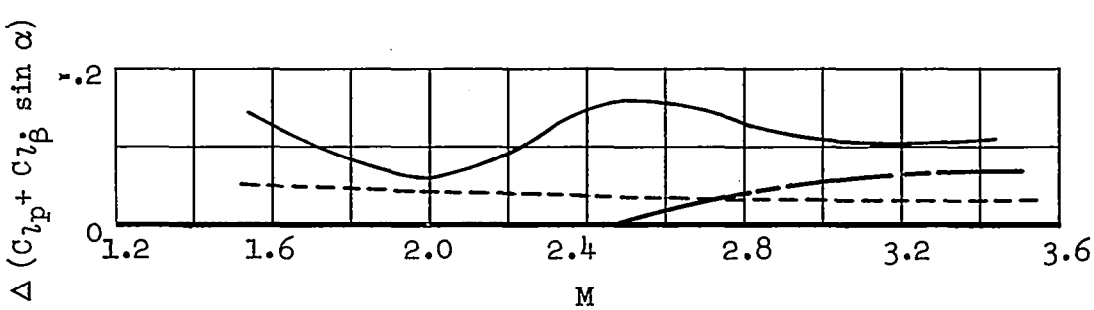

(c) Vertical-tail contribution.

Figure 11.- The variation with Mach number of the damping in roll for the basic configuration both with and without vertical and horizontal tail.

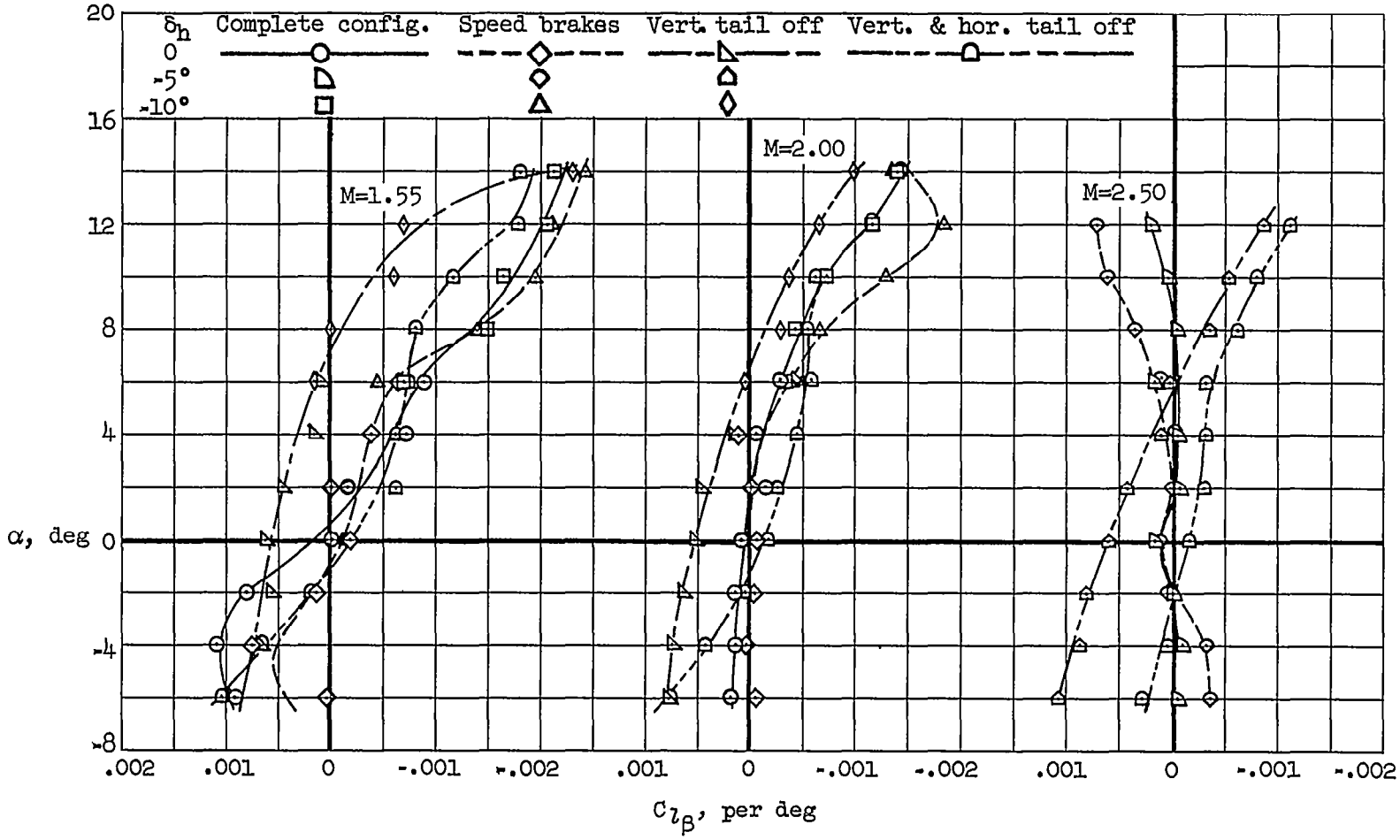

(a) M = 1.55, M = 2.00, M = 2.50

Figure 12.- The variation of the effective dihedral with angle of attack.

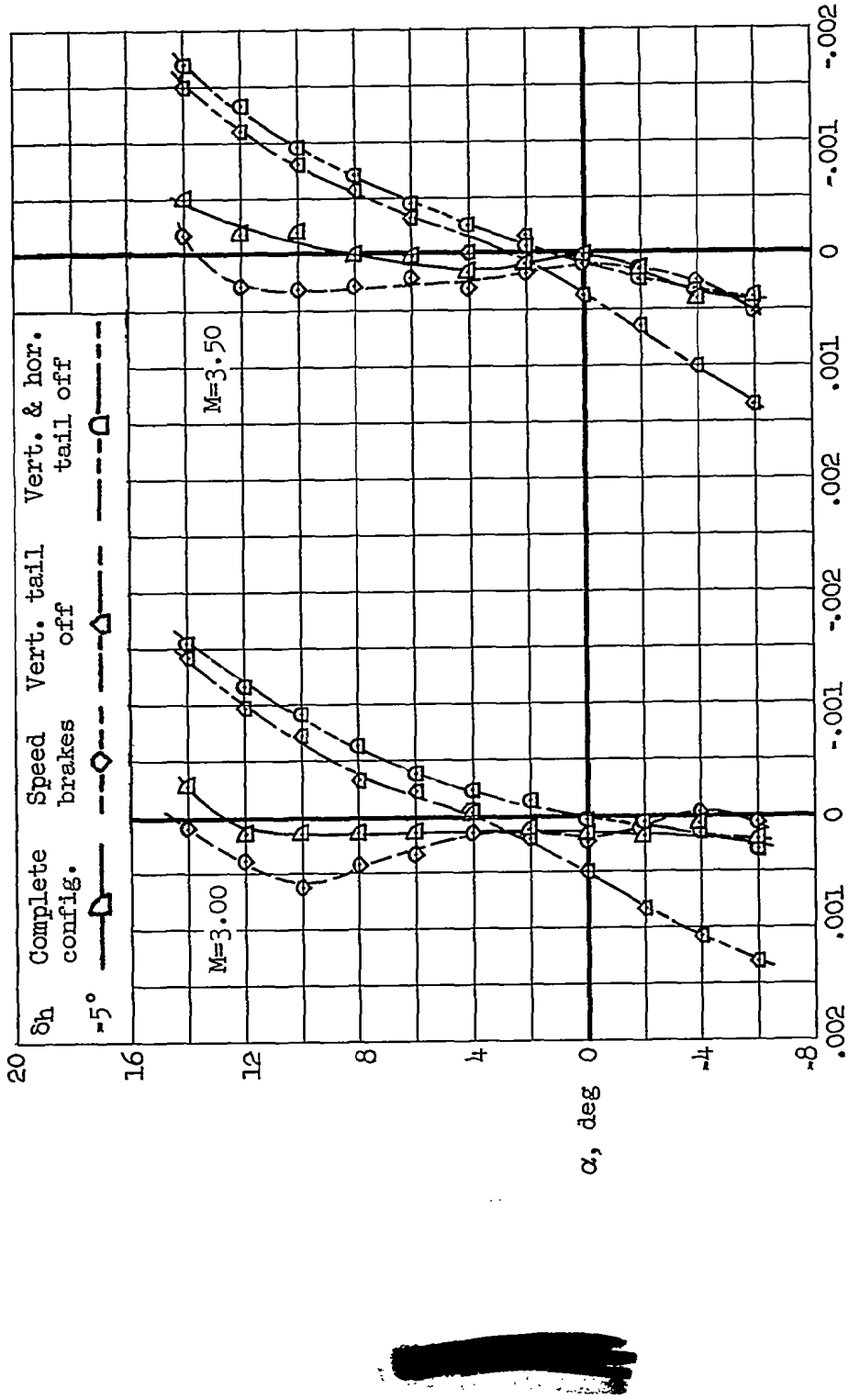

(b) M = 3.00, M = 3.50

Figure 12.- Concluded.

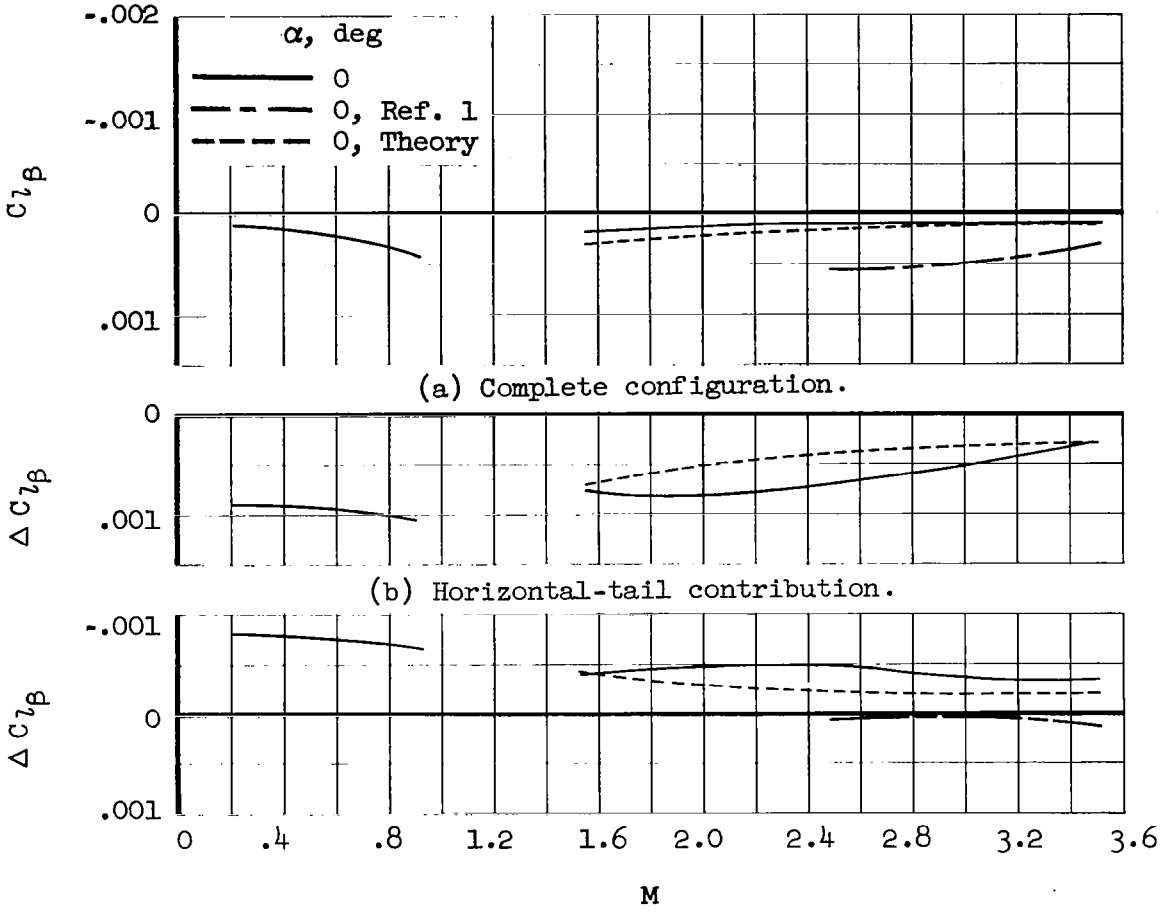

(a) Complete configuration.

(b) Horizontal-tail contribution.

(c) Vertical-tail contribution.

Figure 13.- The variation with Mach number of the effective dihedral for the complete configuration and for the horizontal- and vertical-tail contribution.

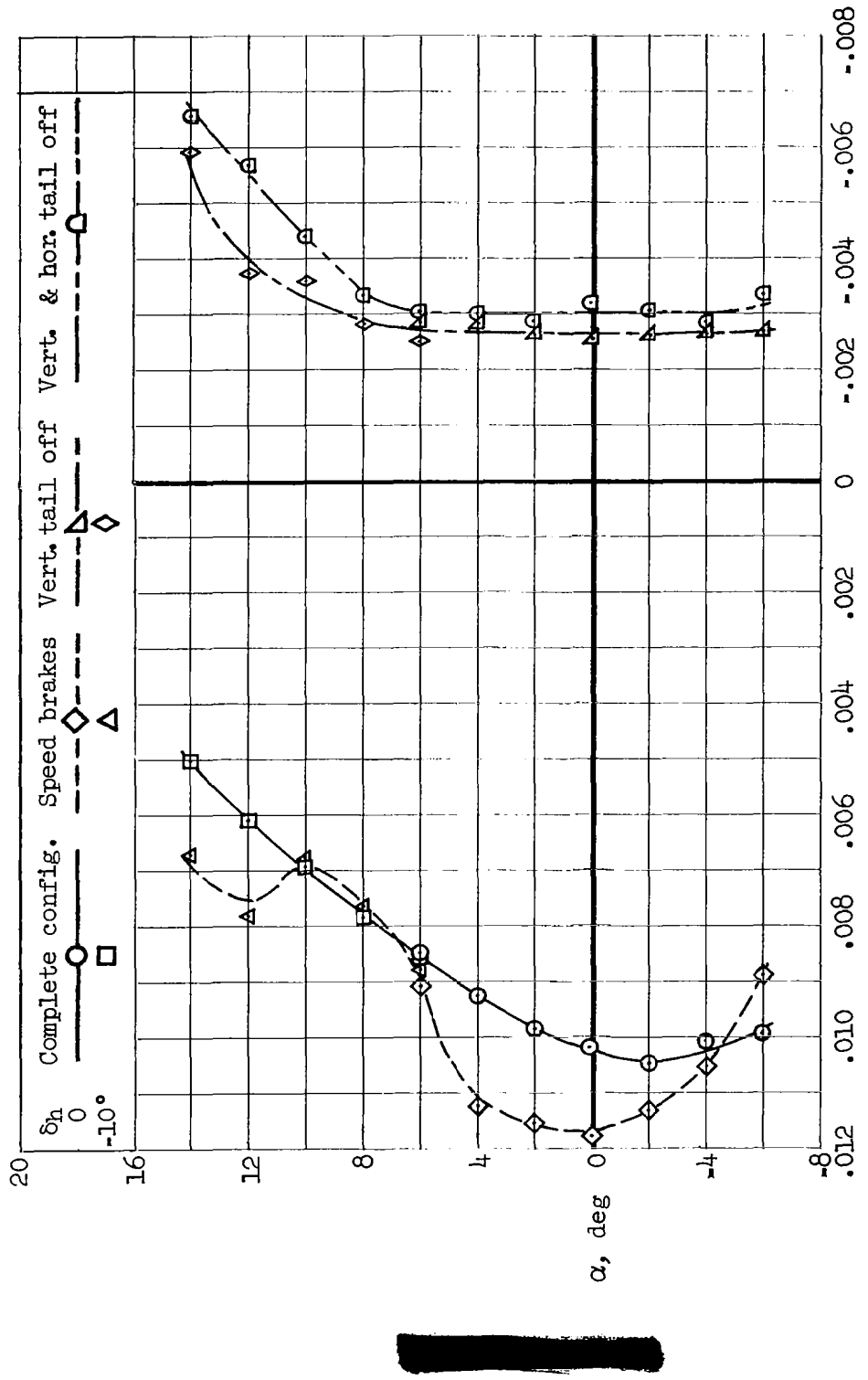

(a) M = 1.55

Figure 14.- The variation of the static directional stability with angle of attack.

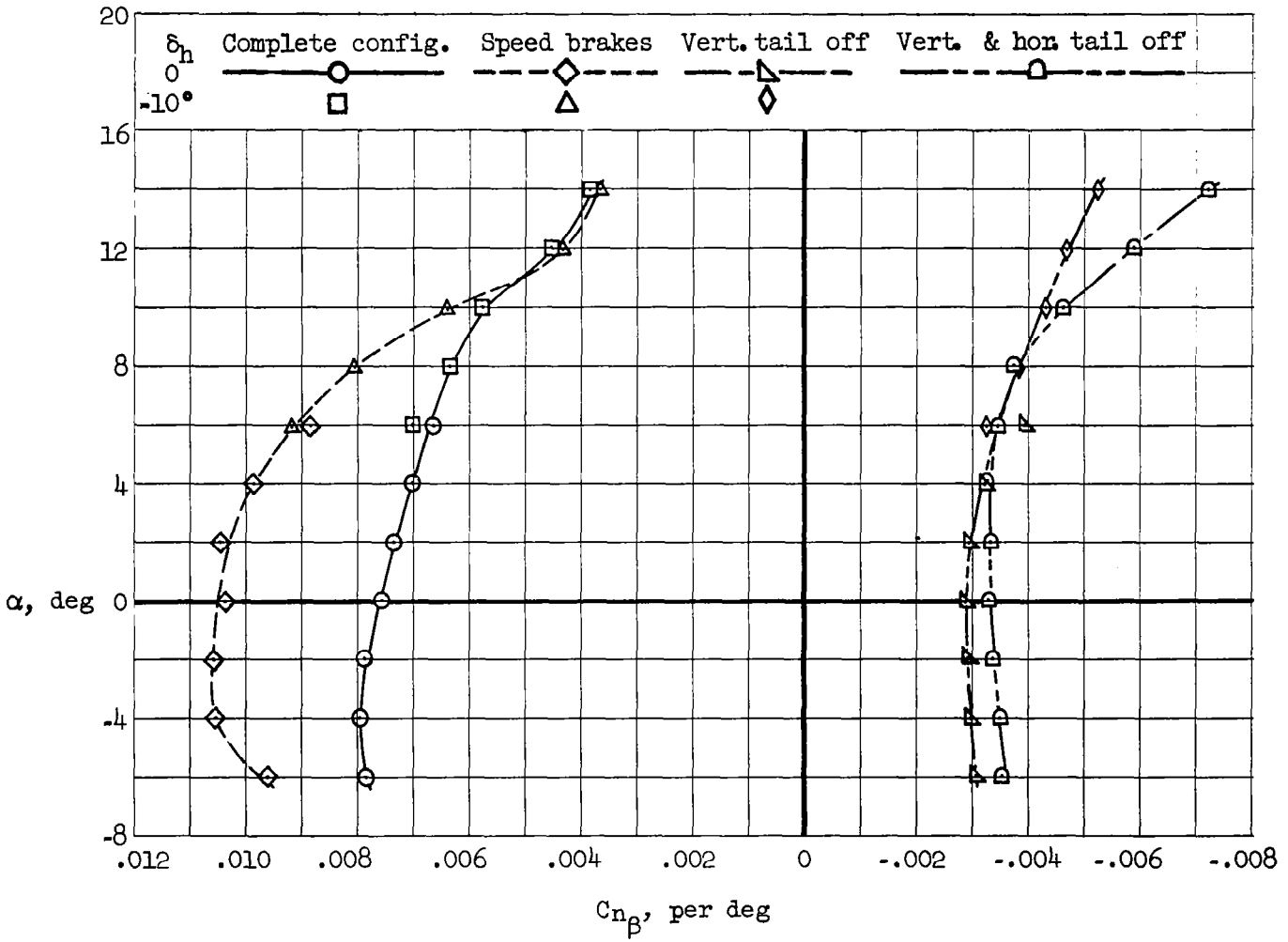

(b) M = 2.00

Figure 14.- Continued.

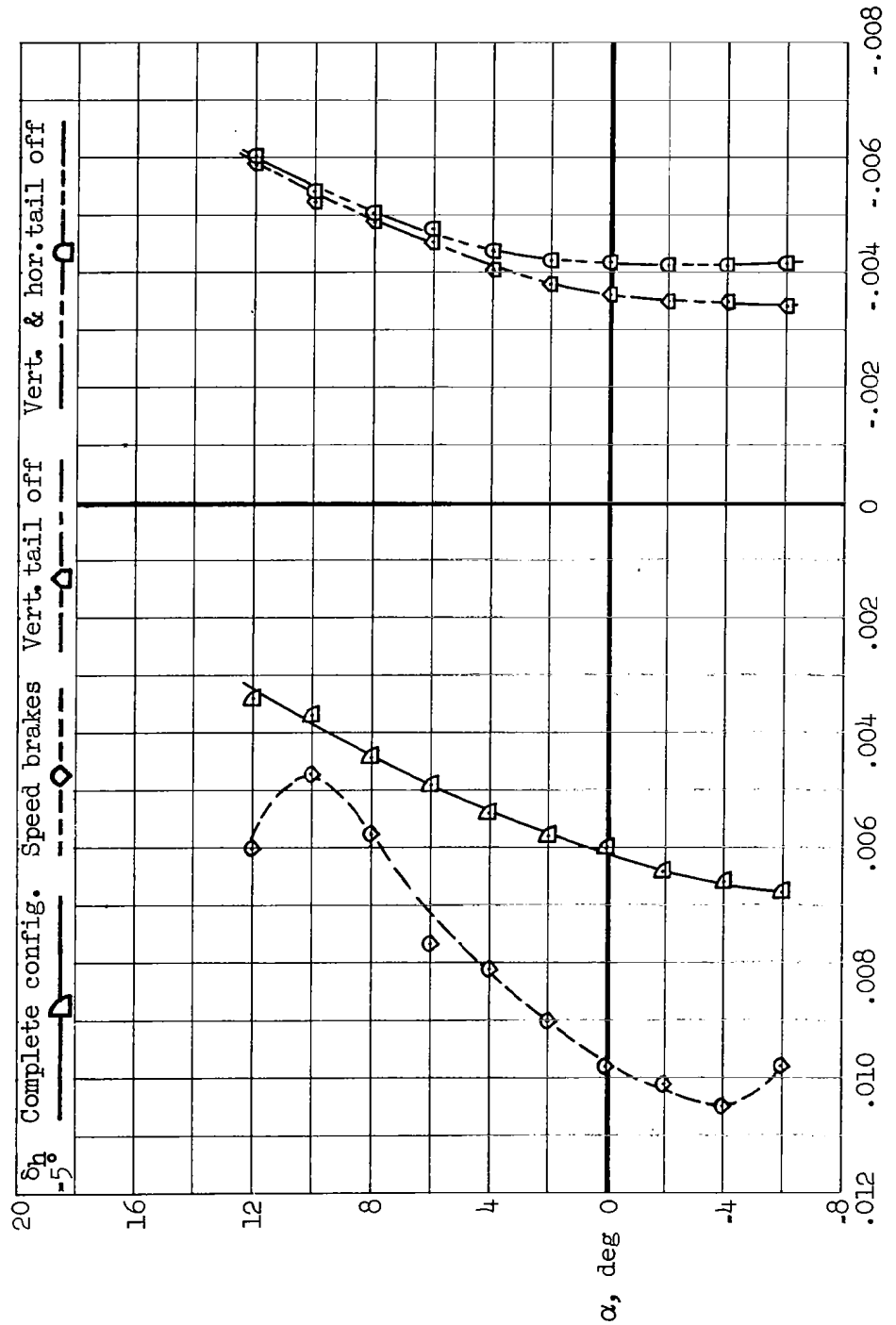

(c) M = 2.50

Figure 14.- Continued.

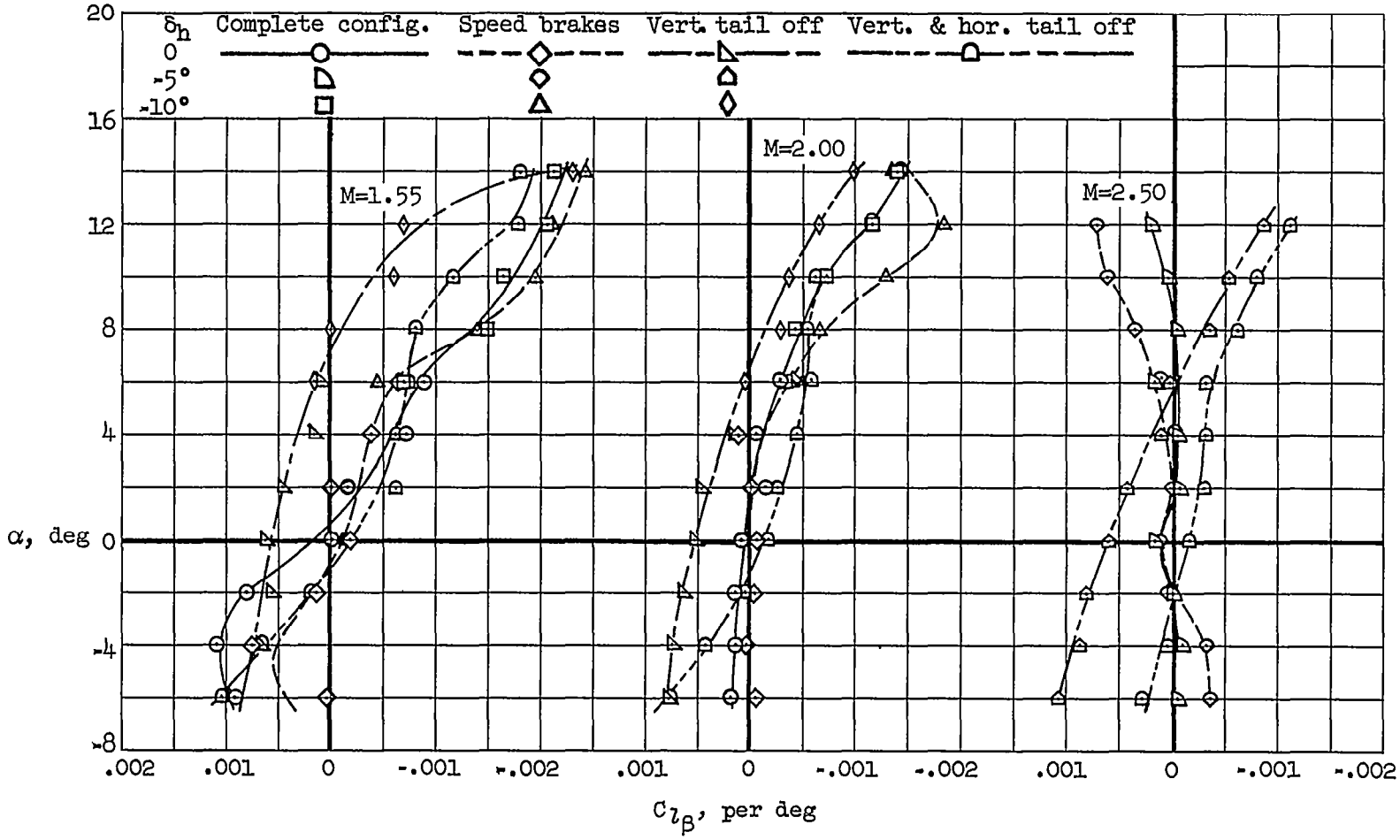

(a) M = 1.55, M = 2.00, M = 2.50

Figure 12.- The variation of the effective dihedral with angle of attack.

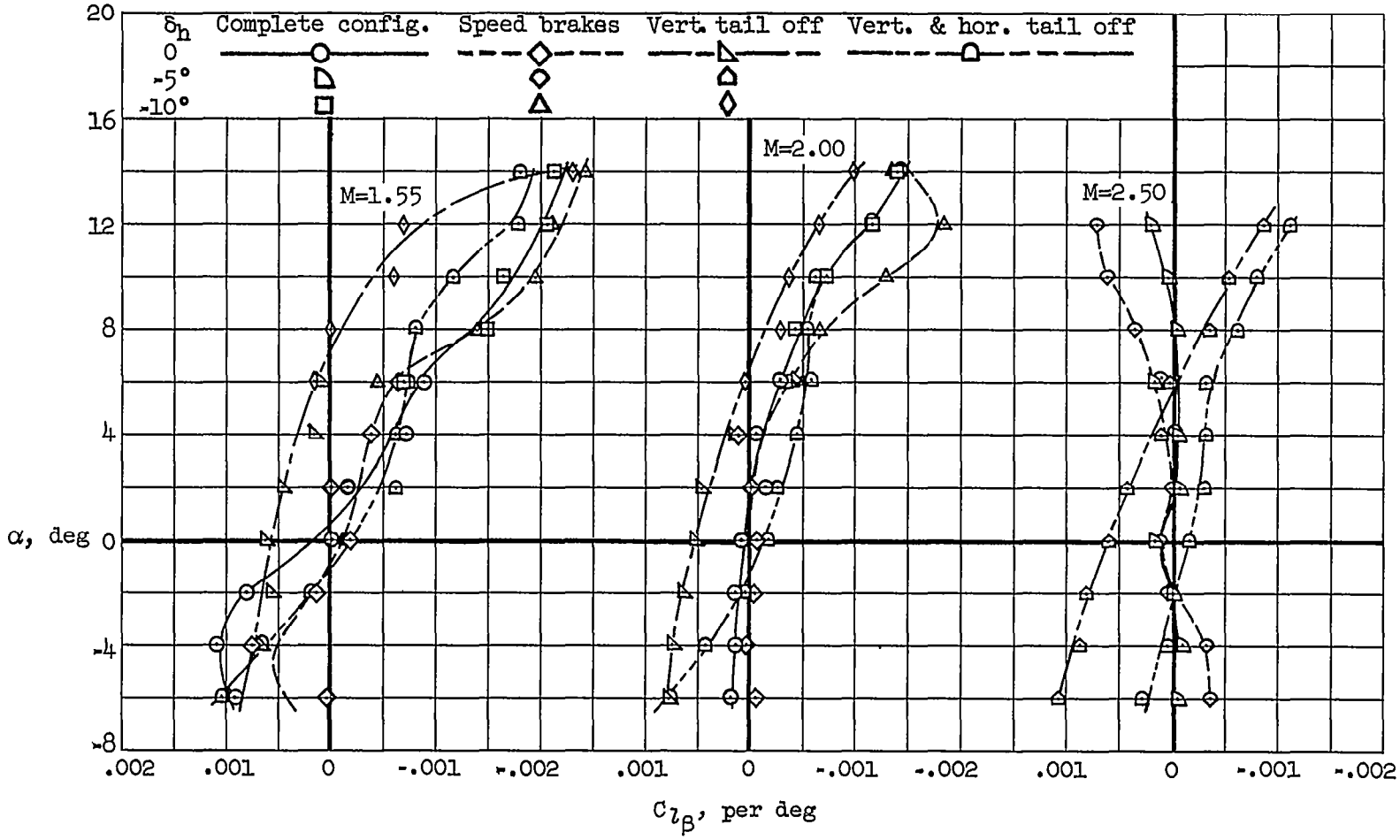

(a) M = 1.55, M = 2.00, M = 2.50

Figure 12.- The variation of the effective dihedral with angle of attack.

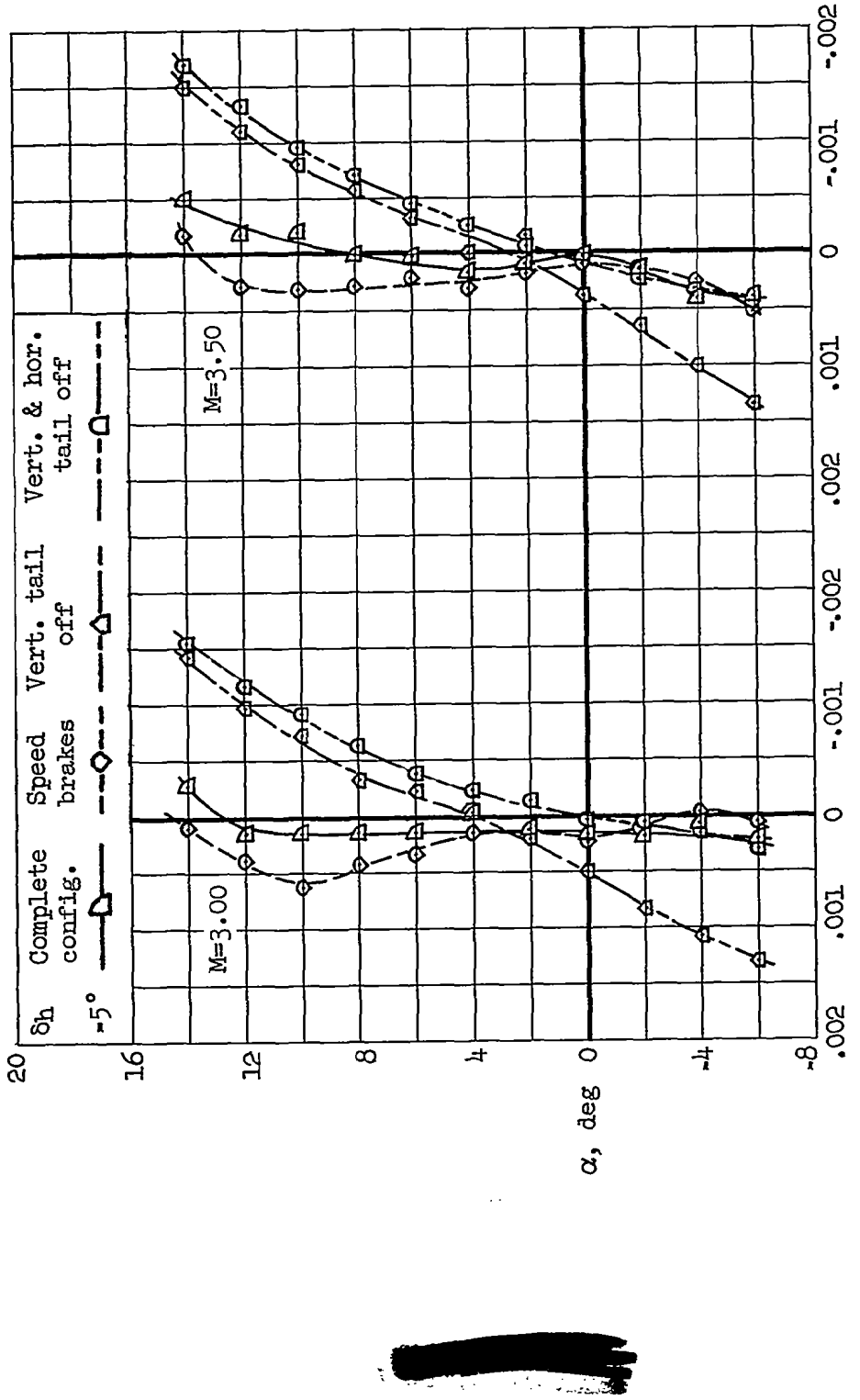

(b) M = 3.00, M = 3.50

Figure 12.- Concluded.

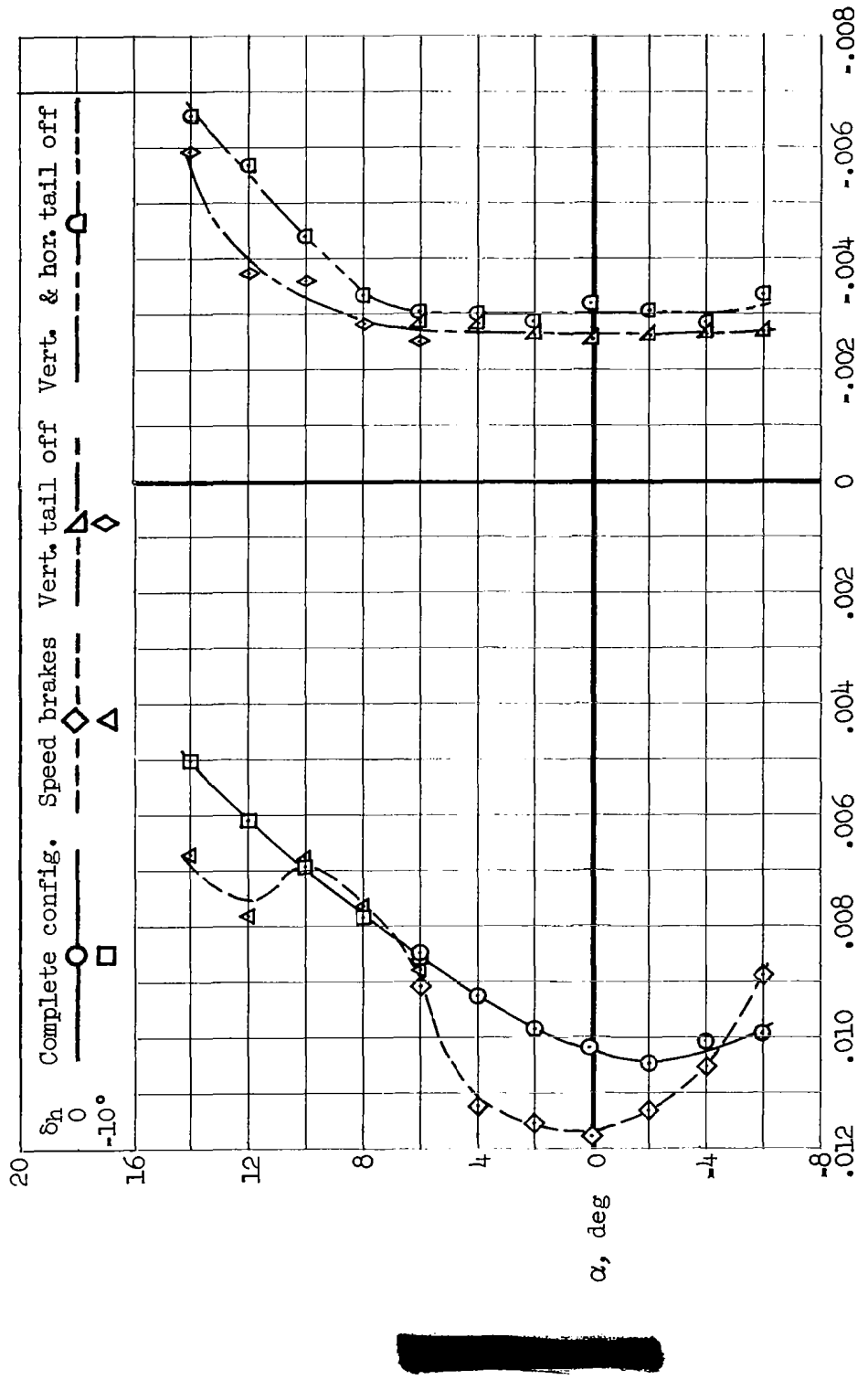

(a) M = 1.55

Figure 14.- The variation of the static directional stability with angle of attack.

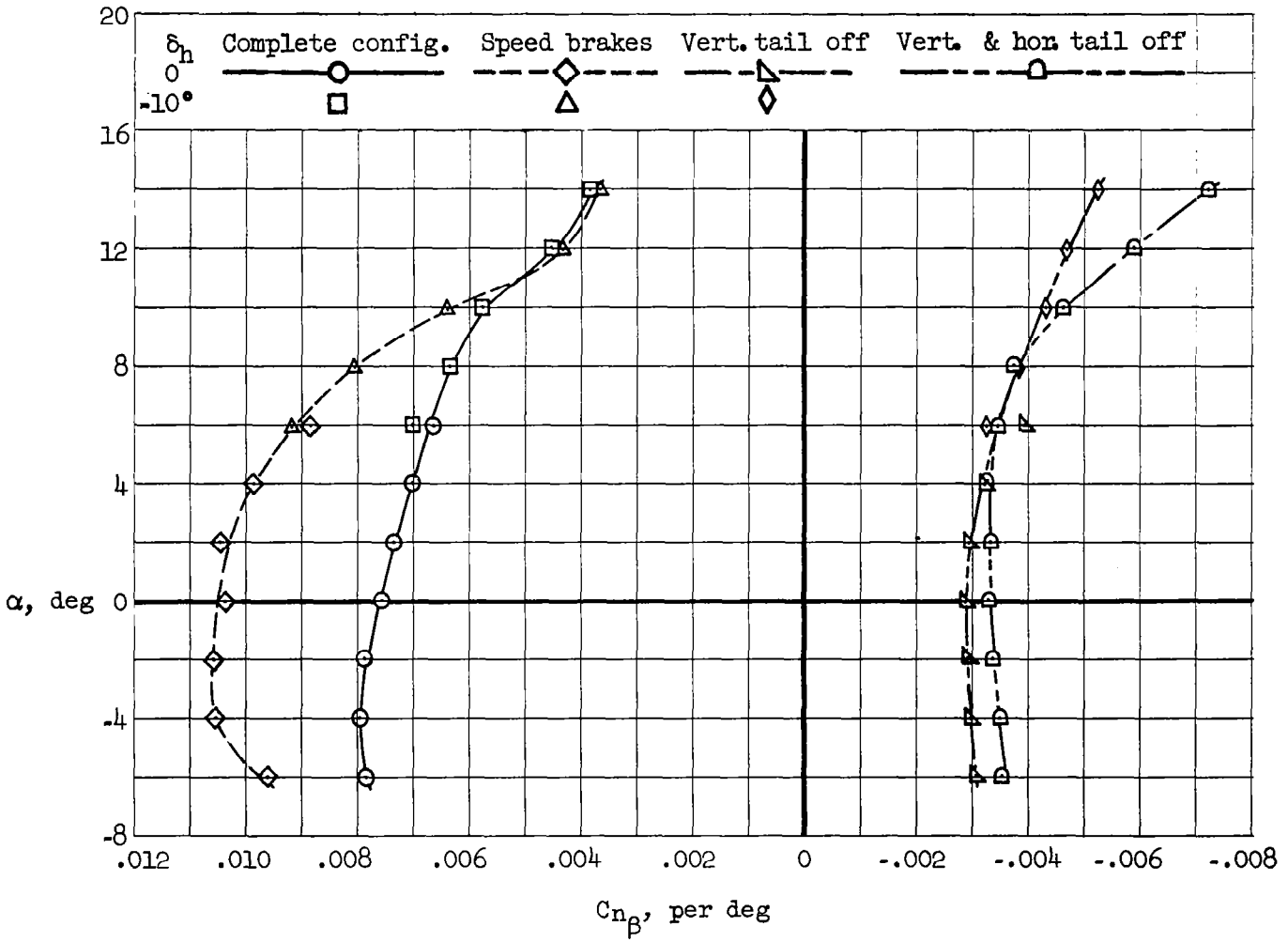

(b) M = 2.00

Figure 14.- Continued.

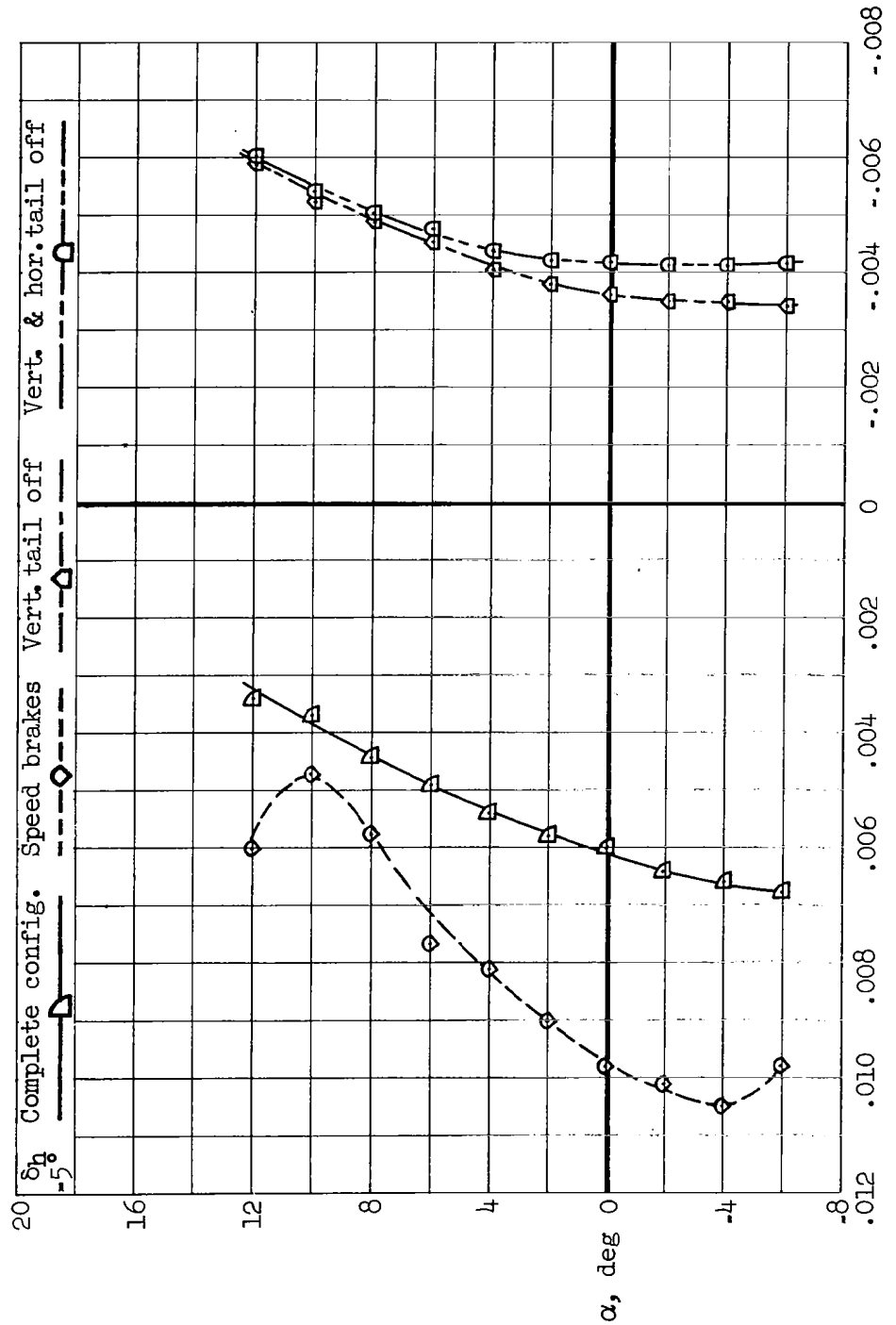

(c) M = 2.50

Figure 14.- Continued.

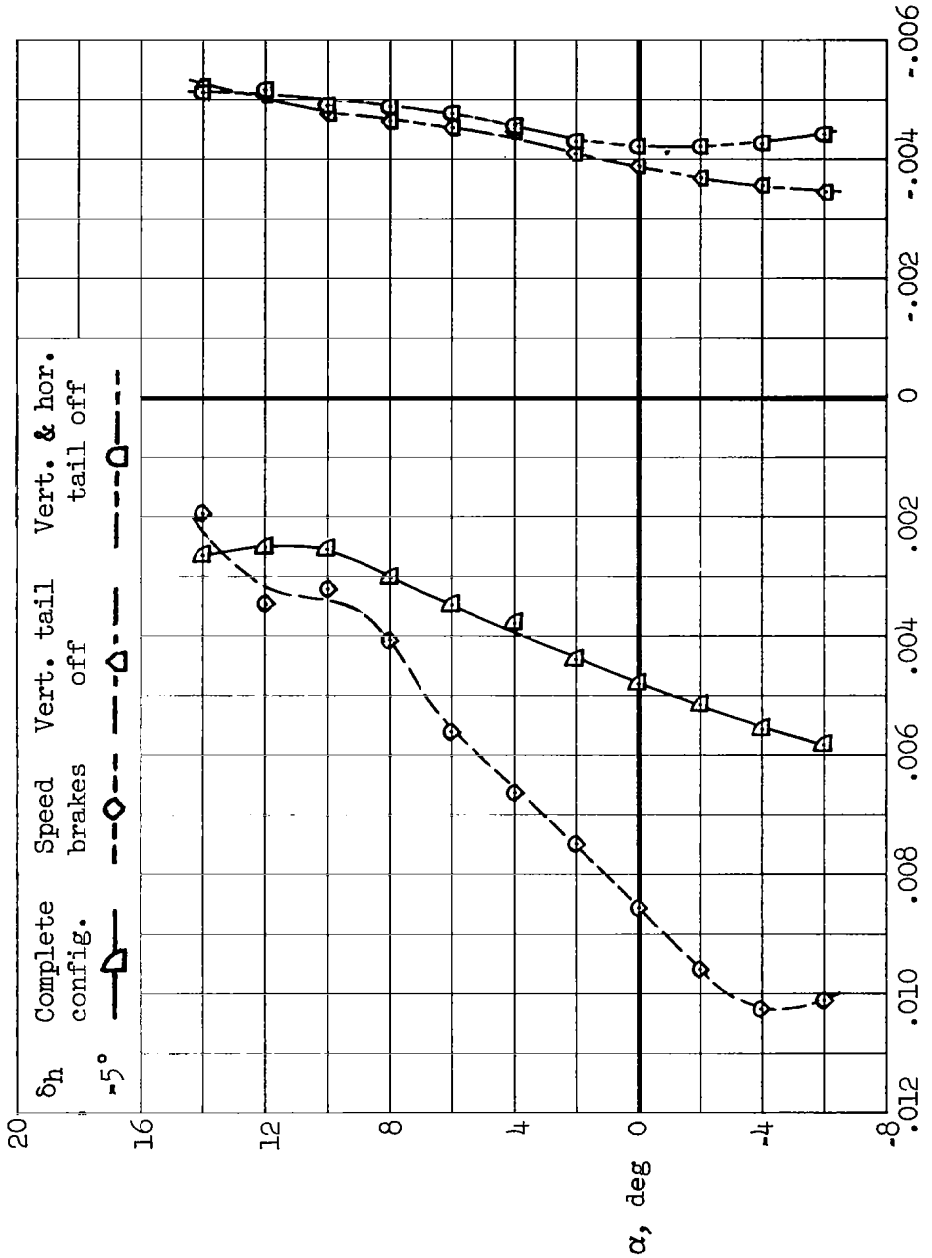

(d) M = 3.00

Figure 14.- Continued.

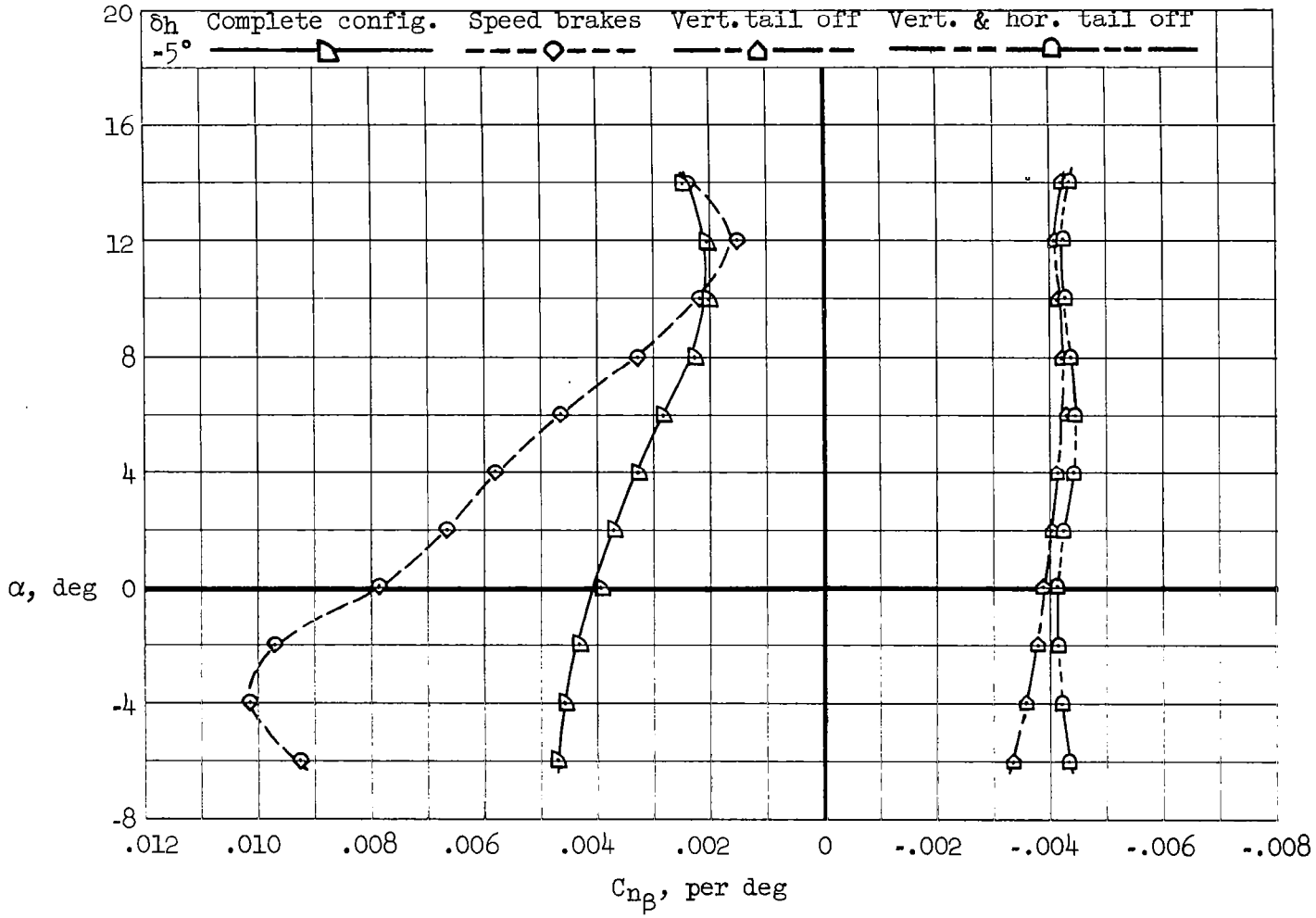

(e) M = 3.50

Figure 14.- Concluded.

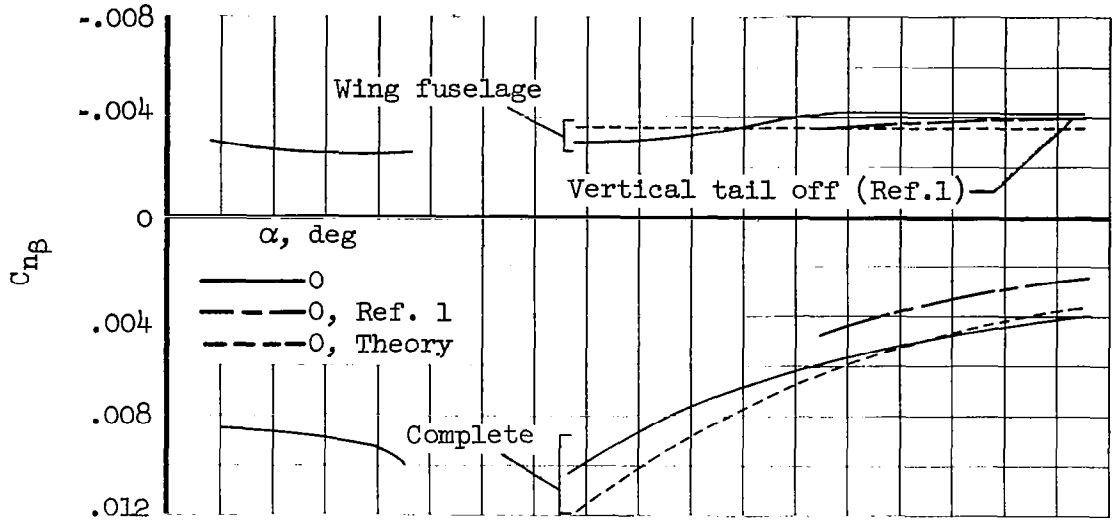

(a) Complete configuration and wing fuselage.

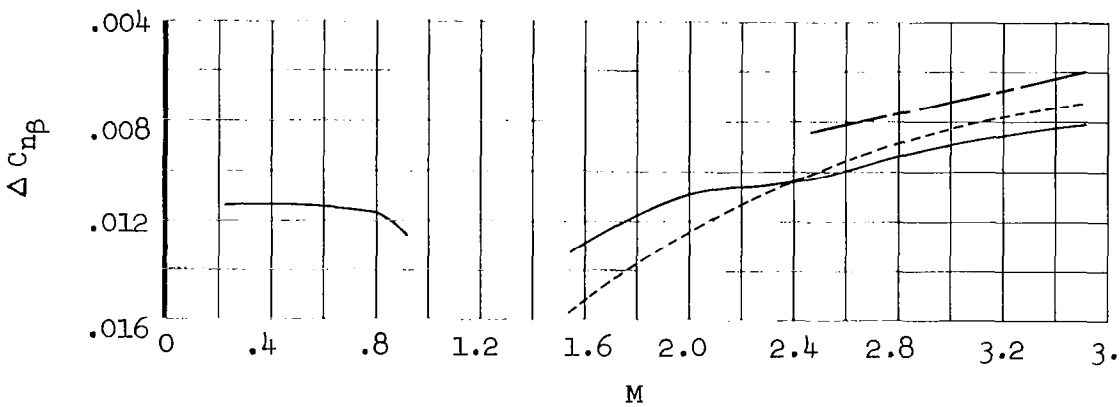

(b) Vertical-tail contribution.

Figure 15.- The variation with Mach number of the static directional stability for the complete configuration both with and without the vertical and horizontal tails.